



January 2012

## Investigating Elevated Aqua Modis Aerosol Optical Depth Retrievals Over The Mid-Latitude Southern Oceans

Travis Toth

[How does access to this work benefit you? Let us know!](#)

Follow this and additional works at: <https://commons.und.edu/theses>

---

### Recommended Citation

Toth, Travis, "Investigating Elevated Aqua Modis Aerosol Optical Depth Retrievals Over The Mid-Latitude Southern Oceans" (2012). *Theses and Dissertations*. 1383.

<https://commons.und.edu/theses/1383>

This Thesis is brought to you for free and open access by the Theses, Dissertations, and Senior Projects at UND Scholarly Commons. It has been accepted for inclusion in Theses and Dissertations by an authorized administrator of UND Scholarly Commons. For more information, please contact [und.commons@library.und.edu](mailto:und.commons@library.und.edu).

INVESTIGATING ELEVATED AQUA MODIS AEROSOL OPTICAL  
DEPTH RETRIEVALS OVER THE MID-LATITUDE  
SOUTHERN OCEANS

by

Travis Dean Toth  
Bachelor of Science, Millersville University, 2010

A Thesis

Submitted to the Graduate Faculty

of the

University of North Dakota

in partial fulfillment of the requirements

for the degree of

Master of Science

Grand Forks, North Dakota  
December  
2012

Copyright 2012 Travis D. Toth

This thesis, submitted by Travis D. Toth in partial fulfillment of the requirements for the Degree of Master of Science from the University of North Dakota, has been read by the Faculty Advisory Committee under whom the work has been done and is hereby approved.



---

Dr. Jianglong Zhang, Chairperson



---

Dr. Cedric Grainger, Committee Member



---

Dr. Jeffrey Reid, Committee Member

This thesis is being submitted by the appointed advisory committee as having met all of the requirements of the Graduate School at the University of North Dakota and is hereby approved.

---

Dr. Wayne Swisher,  
Dean of the Graduate School

---

Date


PERMISSION

Title            Investigating Elevated Aqua MODIS Aerosol Optical Depth Retrievals  
                    Over the Mid-Latitude Southern Oceans

Department    Atmospheric Sciences

Degree         Master of Science

In presenting this thesis in partial fulfillment of the requirements for a graduate degree from the University of North Dakota, I agree that the library of this University shall make it freely available for inspection. I further agree that permission for extensive copying for scholarly purposes may be granted by the professor who supervised my thesis work or, in their absence, by the chairperson of the department or the dean of the Graduate School. It is understood that any copying or publication or other use of this thesis or part thereof for financial gain shall not be allowed without my written permission. It is also understood that due recognition shall be given to me and to the University of North Dakota in any scholarly use which may be made of any material in my thesis.

Signature: 

Date: December 6, 2012

## TABLE OF CONTENTS

LIST OF FIGURES.....	vii
LIST OF TABLES.....	x
ACKNOWLEDGEMENTS .....	xi
ABSTRACT .....	xii
CHAPTER	
I. INTRODUCTION.....	1
II. DATA AND METHODOLOGY.....	10
Ground-Based Observations.....	10
Passive Satellite Observations.....	11
Active Satellite Observations.....	13
Collocation Method and Collocated Data Subsets.....	15
The Spatial Representativeness Problem.....	23
III. RESULTS AND DISCUSSION .....	27
Analysis of Ground-Based AOD Observations.....	27
CALIOP/Aqua MODIS Collocated Analyses.....	29
CALIOP_Cloud Subset Analysis.....	30
CALIOP_Aerosol Subset Analysis.....	42
Spatial Representativeness Analysis.....	50
Seasonal Analysis.....	51
A Case Study.....	53

IV. SUMMARY AND CONCLUSIONS.....	56
APPENDIX .....	60
REFERENCES .....	62

## LIST OF FIGURES

Figure	Page
1. Spatial plots of AOD from various passive satellite datasets (a-c, e-g) and an active dataset (d) show the presence of ESOA in some and its absence in others. A zonal plot of Maritime Aerosol Network (MAN) AOD (h) provides a ground-based perspective of this phenomenon.....	5
2. The spatial collocation of CALIOP and Aqua MODIS datasets. In this example, there are two 5-km CALIOP segments for one 10x10 km MODIS retrieval.....	16
3. The horizontal and vertical resolutions of a 5-km CALIOP L2_VFM file (duplicated from the CALIPSO Quality Statements webpage, <a href="http://eosweb.larc.nasa.gov/PRODOCS/calipso/Quality_Summaries/CALIOP_L2VFMProducts_3.01.html">http://eosweb.larc.nasa.gov/PRODOCS/calipso/Quality_Summaries/CALIOP_L2VFMProducts_3.01.html</a> , retrieved on December 5, 2012).....	20
4. Scatterplot of Maritime Aerosol Network (MAN) AOD vs. Aqua MODIS (AM) AOD for 2004 to 2011 for latitudes south of 40°S. The one-to-one line is in gray, and the data points are colored based on AM cloud fraction.....	27
5. Scatterplots of Aerosol Robotic Network (AERONET) AOD vs. Aqua MODIS (AM) AOD for 2007 to 2009 at (a) Dunedin and (b) Crozet. The one-to-one lines are in gray, and the data points are colored based on AM cloud fraction.....	28
6. From 2007-2009, (a) AM-100 Aqua MODIS Collection 5.1 global mean AOD from over-ocean ‘marginal’, ‘good’, and ‘very good’ datasets and (b) their respective data counts, both displayed at 1.0° x 1.0° resolution.....	31
7. From 2007-2009, (a) AM-0 and (b) AM-CALIOP Aqua MODIS Collection 5.1 global mean AOD from over-ocean ‘marginal’, ‘good’, and ‘very good’ datasets, displayed at 1.0° x 1.0° resolution.....	32
8. Three-year (2007-2009) global zonal mean of AM-100, AM-80, AM-0, and AM-CALIOP Aqua MODIS Collection 5.1 AOD datasets represented spatially in Figs. 6 and 7.....	33
9. Three-year (2007-2009) global zonal mean of CALIOP VFM classification percentages from the AM-100 and AM-0 CALIOP_Cloud analyses.....	34



10. Three-year (2007-2009) global zonal mean of percentage of residual cloud plotted with the relative percentages of particular type of residual cloud in the AM-0 sample.....	36
11. Three-year (2007-2009) CALIOP VFM classification percentages as a function of AM AOD from AM-100 and AM-0 CALIOP_Cloud analyses for the globe...37	37
12. Three-year (2007-2009) CALIOP VFM classification percentages as a function of AM AOD from the AM-100 and AM-0 CALIOP_Cloud analyses for the Southern Oceans.....	38
13. Three-year (2007-2009) relative CALIOP sub-classification percentages of the “Other” classification (shown in Fig. 12) as a function of AM AOD.....	38
14. Vertical distribution of features classified by CALIOP VFM from the AM-100 and AM-0 CALIOP_Cloud analyses as a function of (a) height and (b) temperature using two classification schemes. See the text for the differences between the two schemes.....	40
15. From 2007-2009, (a) AM-100, (b) AM-0 and (c) AM-CALIOP global mean CALIOP AOD for the CALIOP_Aerosol subset analysis at 1.0° x 1.0° resolution.....	42
16. Three-year (2007-2009) global zonal mean of (a) Aqua MODIS AOD (in blue) and the respective CALIOP AOD (in red) for the CALIOP_Aerosol subset analysis, and (b) the AOD differences between Aqua MODIS and CALIOP for AM-100 (in purple), AM-0 (in green), and AM-CALIOP (in yellow).....	44
17. Scatter plot of the change in zonal mean CALIOP cloud fraction (as determined from the VFM) versus the change in zonal mean Aqua MODIS AOD from the AM-100 and AM-0 CALIOP_Aerosol subset analyses.....	46
18. Three-year (2007-2009) average frequency of occurrence of (a) VFM classification categories, (b) “Other” subcategory classification, and (c) “Both” subcategory classification, and their respective Aqua MODIS and CALIOP AOD for the AM-100 CALIOP_Aerosol subset analysis for the Southern Oceans. Figure (d) depicts the differences in Aqua MODIS and CALIOP AOD between the “Other” and “Both” subcategories.....	47
19. Three-year (2007-2009) average frequency of occurrence of (a) VFM classification categories, (b) “Other” subcategory classification, and (c) “Both” subcategory classification, and their respective Aqua MODIS and CALIOP AOD for the AM-0 CALIOP_Aerosol subset analysis for the Southern Oceans. Figure (d) depicts the differences in Aqua MODIS and CALIOP AOD between the “Other” and “Both” subcategories.....	48

20. Three-year (2007-2009) global zonal mean of AM-CALIOP Aqua MODIS AOD from the CALIOP\_Aerosol analysis. Original is in dark blue and the corresponding renormalized AOD is in orange and green (based on slightly different AOD averaging schemes).....51

21. Three-year (2007-2009) global zonal mean of Aqua MODIS AOD (in blue) and the respective CALIOP AOD (in red) for the southern hemisphere (a) summer months (November through April, or NDJFMA) and (b) winter months (May through October, or MJJASO).....52

22. Case study of a collocated Aqua MODIS (AM) and CALIOP point (-50.6°, -18.7°) on January 12<sup>th</sup>, 2009 at 15:26 UTC. A visible image of AM is shown in (a), where the red line indicates the CALIOP track, the blue box shows the 10x10 km AM-0 retrieval, and the black arrow points to the midpoint of the 5 km CALIOP segment. (b) The corresponding AM AOD spatial plot. (c) CALIOP Vertical Feature Mask (VFM) plot. (d) Line plot of AM AOD, AM cloud fraction, and CALIOP AOD.....54

## LIST OF TABLES

Table	Page
1. CALIPSO products and parameters utilized in this study.....	15
2. The criteria for each subset analysis and their respective products.....	23
3. Mean values of Aqua MODIS, MAN, Crozet, and Dunedin AOD for all points in each dataset, as well as only those with a MODIS cloud fraction of 0%.....	29
4. For the CALIOP_Cloud and CALIOP_Aerosol analyses, each subset is described (AM-100, AM-0, and AM-CALIOP), and corresponding data point samples and mean Southern Oceans AOD are reported for the 2007-2009 time period of this study.....	30
5. For the CALIOP_Aerosol analysis, data counts in the Southern Oceans region for each subset analysis (AM-100, AM-0, and AM-CALIOP) for the southern hemisphere summer months (November through April, or NDJFMA) and winter months (May through October, or MJJASO) are reported.....	53

## ACKNOWLEDGEMENTS

Thank you to my advising committee of Drs. Jianglong Zhang, Cedric Grainger, and Jeffrey Reid for their continual guidance and support throughout the course of this thesis work. Thank you to all of my family and friends for their encouragement, love, and support. Thank you to all of the graduate students in the Atmospheric Sciences Department for the fun times during my graduate school experience, especially those in my research group. Special thanks to Yingxi Shi and Randall Johnson for their help with computer programming, data, and figures.

The Office of Naval Research Codes 32 and 35, Office of Naval Research Young Investigator Program, and NASA Interdisciplinary Science Program funded this research. The CALIPSO data (Drs. David Winker and Mark Vaughan) were obtained from NASA Langley Research Center Atmospheric Science Data Center. The MODIS data were obtained from NASA Goddard Space Flight Center. The AERONET program and their contributing principal investigators and their staff are acknowledged and appreciated for establishing and maintaining the AERONET sites used in this investigation. Dr. Alexander Smirnov is acknowledged and appreciated for providing the MAN data utilized for this project, and Dr. James Campbell is thanked for his guidance and expertise.

## ABSTRACT

A band of elevated aerosol optical depth (AOD) over the mid-latitude Southern Oceans has been identified in some passive satellite-based aerosol datasets such as Moderate Resolution Imaging SpectroRadiometer (MODIS) and Multi-angle Imaging SpectroRadiometer (MISR) products. In this study, Aqua MODIS (AM) aerosol products in this zonal region are investigated in detail to assess retrieval accuracy. This is done through multiple data sets, including spatially and temporally collocated cloud and aerosol products produced by the Cloud-Aerosol Lidar with Orthogonal Polarization (CALIOP) project for investigating AM AOD in this region with respect to lidar profiling of cloud presence. Maritime Aerosol Network (MAN) and Aerosol Robotic Network (AERONET) AOD data are also collocated with AM for surface context. The results of this study suggest that the apparent high AOD belt, seen in some satellite aerosol products based on passive remote sensing methods, is not seen in the CALIOP aerosol product based on an active remote sensing technique with an enhanced cloud detection capability and is not detected from ground-based observations such as MAN and AERONET data. The apparent high AOD belt, although largely attributed to stratocumulus and low broken cumulus cloud contamination as suggested by CALIOP products, could not be fully credited to cloud contamination. Collocated CALIOP data also suggest that the current cloud screening methods implemented in the over ocean AM aerosol products are ineffective in identifying cirrus clouds. Cloud residuals still exist in the AM AOD products even with the use of the most stringent cloud screening settings.

## CHAPTER I

### INTRODUCTION

Atmospheric aerosols are small solid and/or liquid particles suspended in the air (Wallace and Hobbs 2006). They originate from both anthropogenic and natural sources, and include categories such as sulfates, carbonaceous aerosols, dust, and sea salt (SS). With common lifetimes in the atmosphere of a week or less, aerosols have high spatial and temporal variability with concentrations peaking near their source (Ramanathan et al. 2001). With a global presence, aerosols play an important role in the planetary radiation budget, as they reflect and absorb solar radiation (e.g. Ramanathan et al. 2001). Aerosols also serve as cloud condensation nuclei (CCN), affecting the hydrologic cycle by modifying cloud formation and precipitation processes (e.g., Kaufman et al. 2002). Thus, an accurate understanding of their optical and microphysical properties is essential to furthering the current understanding of the global climate system (e.g., Wielicki et al. 1995, Anderson et al. 2003).

Besides climate, there are other important impacts of aerosols. For example, pollution in the atmosphere poses significant risks to human health (Pope 2004). Black carbon and dust are the primary pollutants in Asia, and through atmospheric transport, other continents as well (Menon et al. 2002). Also, the hazy weather conditions induced by aerosols affect atmospheric visibility, and consequently, military operations. Thus scientists affiliated with the U.S. Navy, for example, are largely involved in visibility forecasting by modeling aerosols in marine environments (Gathman et al. 1983). The

accuracy of these forecasts, as well as climate-related research endeavors, depends upon the scientific understanding of the impacts aerosols have on the Earth system. Several measurement techniques have been developed throughout the years to help advance the science of atmospheric aerosols. *In situ* observations of aerosols involve the direct contact of instrumentation with the ambient air, and provide important characteristics of the chemical composition of aerosols (Delene and Ogren 2002). On the other hand, remote sensing observations are taken at some distance away from the aerosols, and include measurements from ground-based and satellite instrumentation. The strength of ground-based remote sensing is that it provides a closer measurement of aerosols and thus is frequently used as ground truth for space-borne remote sensing studies. While the small spatial scale of ground-based remote sensing measurements is a major limitation, satellite observations cover larger areas and provide a unique perspective of the distribution of aerosols across the globe (Purkis and Klemas 2011).

The remote sensing community takes advantage of the global diurnal coverage of satellites to study the Earth's highly variable aerosol distributions through a quantity called the aerosol optical depth (AOD). AOD is a measure of the attenuation of sunlight (by scattering and absorption) in a column of aerosol, and thus provides the vertically integrated aerosol concentration in an atmospheric profile (Kaufman et al. 2002). Therefore, AOD is a parameter heavily used by scientists to demonstrate, from a satellite perspective, the significance of aerosol radiative properties in atmospheric processes.

However, aerosol observations from satellites have limitations, as they are sensitive to a variety of factors and thus introduce uncertainty. As outlined by Myhre et al. (2004), these factors include retrieval algorithm assumptions (i.e., ocean reflectance, gaseous

absorption, and aerosol microphysics) and the quality of input satellite radiances utilized during the aerosol retrieval process (i.e., radiometric uncertainties caused by calibration errors and noise, cloud screening). This uncertainty requires the careful intercomparison of satellite AOD retrievals so that they can be used to validate the performance of global aerosol models.

Myhre et al. (2004) did such an intercomparison by examining oceanic AOD observations from five satellites across an eight-month period (November 1996 to June 1997). They found significant differences in AOD (of a factor of two) between the various satellite datasets for most regions of the world, while some regions, such as the remote oceans in the Southern Hemisphere, exhibited even higher discrepancies. Among some of the other reasons outlined earlier, the main probable cause of this disagreement was suggested to be cloud screening.

A later paper, Myhre et al. (2005), focused on a similar intercomparison of AOD retrievals over global oceans. This time, however, nine datasets were examined and the study period was extended to forty months (September 1997 to December 2000). The differences in AOD between the satellite datasets were found to be even more significant than those discovered from the previous analysis (Myhre et al. 2004). For the later study, cloud screening was not only mentioned, it was discussed in much greater detail. The authors found that, in some cases, the cloud screening protocols were not strict enough and thus causing cloud contamination. However, some cases revealed that the algorithms for cloud screening are too strict, resulting in the misclassification of high AOD retrievals as clouds. Clearly, much work is still necessary to help resolve this issue.



The example studies provided above show that satellite remote sensing of aerosols is a complicated process requiring additional research. The current understanding of the factors mentioned by Myhre et al., 2004 must be advanced in order to increase the accuracy of satellite AOD retrievals. Furthermore, if not properly filtered and/or accommodated for through quality assurance (QA) screening, these systematic biases (caused by signal uncertainty, algorithm bias, cloud contamination, etc.) in satellite AOD datasets can significantly compromise resolution and closure of aerosol radiative and physical processes for future climate investigations (e.g., Zhang et al. 2008; Zhang and Reid 2009).

One unique example of potential signal bias has been found from AOD datasets collected by some passive (i.e., reflecting incident electromagnetic radiation) satellite instruments over the mid-to-high latitude Southern Oceans (defined from 45° S to 65° S), where a band of relatively high AOD is found. The scenario for elevated Southern Oceans AOD (hereafter referred to as ESOA; Gao et al. 2002; Zhang et al. 2005; Zhang and Reid 2006) is depicted in Fig. 1. From 2005, 0.5° x 0.5° averaged AOD from 70° S to 0° S are shown from Collection 5.1 NASA Moderate Resolution Imaging SpectroRadiometer retrievals based on measurements collected aboard the Aqua satellite platform (hereafter referred to as Aqua MODIS or AM; Remer et al. 2005), for over-ocean ‘marginal’ and over-land ‘good’ QA flags, Multi-angle Imaging SpectroRadiometer (MISR) Version 22 retrievals for ‘successful’ QA flags (Diner et al. 1998), Sea-viewing Wide Field-Of View Sensor (SeaWiFS) DeepBlue Level 3 Version 3 (Sayer et al. 2012), and Collection 5.1 Aqua MODIS Level 3 DA-Quality (Zhang et al. 2008), with 1.0° by 1.0° averages shown from Global Aerosol Climatology Project

(GACP; Mishchenko et al. 2007) and Advanced Very High Resolution Radiometer (AVHRR) AERO100 (Rao et al. 1989).

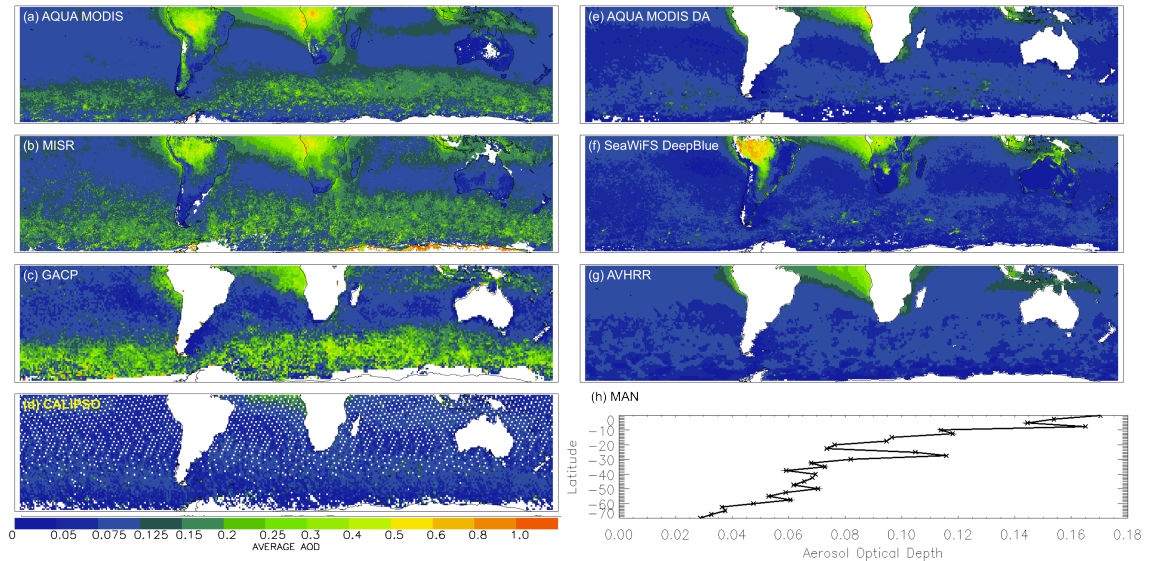


Figure 1. Spatial plots of AOD from various passive satellite datasets (a-c, e-g) and an active dataset (d) show the presence of ESOA in some and its absence in others. A plot of zonally averaged Maritime Aerosol Network (MAN) AOD (h) provides a ground-based perspective of this phenomenon.

ESOA is apparent from three products (Aqua MODIS, MISR, and GACP), while the others (Aqua MODIS DA, SeaWiFS DeepBlue, and AVHRR) do not exhibit similar structure. The difference is believed to be primarily the result of more stringent cloud screening applied to the Aqua MODIS DA, SeaWiFS Deep Blue and AVHRR datasets, such as the “buddy check” system of investigating single data points relative to surrounding ones as an additional and conservative cloud filtering step (e.g., Zhang and Reid 2006; Shi et al. 2011).

Taking an initial look into ESOA from an active (i.e., transmitting power) remote sensing perspective, Fig. 1d shows 1.0° by 1.0° three-year (2007-2009) averaged AOD from the NASA Cloud-Aerosol Lidar with Orthogonal Polarization (CALIOP; Winker et al. 2007; Hunt et al. 2009) for the same latitude bands (70° S to 0° S) as the other plots in

Fig. 1. Details in constructing Fig. 1d are discussed in the later parts of the thesis. Also, data from 2005 are used to generate AOD spatial distributions from passive sensors (Figs. 1a-1c and 1e-1g), as the GACP and AVHRR data are only available to the public up to 2006 (personal communication with Dr. Jianglong Zhang 2012). The years 2007-2009 are used to generate Fig. 1d using CALIOP data, as there is no CALIOP data available prior to June 2006. In a similar manner as Aqua MODIS DA, SeaWiFS DeepBlue, and AVHRR, CALIOP does not detect the presence of ESOA. As such, the initial investigation of ESOA is furthered using a limited amount of data from the Maritime Aerosol Network (MAN; Smirnov et al. 2011). Fig. 1h shows  $2.5^\circ$  zonally averaged MAN AOD values from 2004 to 2011 are less than 0.08 across the Southern Ocean latitudes, and thus ESOA is not indicated by surface observations. Clearly, discrepancies in aerosol loading over the Southern Oceans are observed among passive and active sensors, as well as MAN data, and therefore such discrepancies need to be carefully explored.

Recent research projects have provided several possible causes of the high AOD retrievals reported by some passive satellites in the Southern Oceans region. Some studies suggest that ESOA could be induced by high concentrations of SS aerosols due to strong near surface ocean wind speeds associated with the “Roaring Forties” along this latitudinal band. SS is often the primary component of marine aerosols in this secluded oceanic area (Murphy et al. 1998), as it is far removed from continental and anthropogenic sources (Lewis and Schwartz 2004).

An example study in which ESOA is investigated as a function of wind speed is Zhang and Reid 2006, as they showed that MODIS optical depth algorithms

underestimated AOD in high-wind conditions. They suspected this effect might be due to white foams and larger glint regions, which are found during increases in near-surface wind speeds. In a similar study, Lehahn et al. 2010 shows a band of high wind speeds and AOD in the Southern Hemisphere mid-latitude oceans. Following the results of Zhang and Reid 2006, Lehahn et al. 2010 exclude this “Roaring Forties” region from their analysis in order to consider only the most confident aerosol retrievals.

Madry et al. 2011 also mention ESOA, as their sea salt aerosol modeling efforts estimated AOD to be over 0.2 for the Southern Oceans region. High wind speeds were given as the primary reason behind this phenomenon. While the findings of these studies are important and should be noted, some discrepancy in the relationship between wind speed and ESOA exists. For instance, Fig. 1h, as well as Smirnov et al. (2011), showed that more than 90% of MAN data between 40 and 60° S have AOD values less than 0.1 and 80% of them have AOD values less than 0.05. Thus, it is likely wind speed alone does not cause ESOA.

Another possible contributor to ESOA is the effect of a “Twilight” zone surrounding a cloud, the transitional area between a cloud and the cloud-free atmosphere and aerosols (Koren et al. 2007). Enhanced reflectance in this zone, caused by evaporating cloud fragments and humidified aerosols, can consequently enhance AOD measured in the visible and near-infrared spectrums. These increased values of AOD are observed by passive satellite retrievals, such as MODIS, and ground-based AEROSOL ROBOTIC NETWORK (AERONET) instrumentation. It is estimated that 30-60% of the “cloud-free” atmosphere is affected by this “Twilight” zone, and thus has implications for studies concerning global aerosol forcing (Koren et al. 2007).

Other possible causes of EOSA are inaccurate aerosol models and under/overestimated ocean surface albedo values used in the MODIS retrieval process (Shi et al. 2011), and cloud-sidescattering effects (e.g., Zhang and Reid 2006; Wen et al. 2007; Marshak et al. 2008). The Wen et al. (2007) study focused on 3D aerosol/cloud interaction, observed from MODIS images of cumulus clouds fields. They found that this interaction enhances reflectance of the clear regions near clouds. In a similar study, Marshak et al. (2008) develop a model that is used to quantify the enhanced reflectance of cloud free areas near the presence of clouds. Also, Zhang and Reid (2006) discuss this sidescattering in regards to glint adjacency effects, as more reflected light could be scattered into the region of the AOD satellite retrieval.

Yet another potential contributor to ESOA is cloud contamination of satellite aerosol retrievals. Zhang and Reid (2005) looked into the relationship between MODIS AOD and cloud fraction in remote marine environments, as reported by past research initiatives. They found that the vast majority (60-90%) of this relationship is the result of cloud contamination and cloud brightening effects, and suggest that these artifacts may partially contribute to the high values of AOD observed over the Southern Oceans region. Similar conclusions were found by a later study, Zhang and Reid (2006), during which biases in over-ocean MODIS AOD retrievals were explored to improve aerosol data assimilation. By removing biases due to cloud artifacts, the authors discovered a global decrease in MODIS AOD of 0.018 (0.145 to 0.127, or ~12%), with a 30% reduction occurring across the Southern Oceans. These results are consistent with Kaufman et al. 2005, as they found cloud contamination increased MODIS AOD by 0.02 (0.13 to 0.15, or ~15%).

The research presented in this thesis aims to build upon these studies by not only quantifying the enhancement of AOD by clouds, but also determining what clouds have the greatest contribution to this contamination. While there are numerous possible contributors to ESOA, this study focuses on cloud contamination. ESOA, as detected by Aqua MODIS, is first evaluated using collocated ground-based observations, followed by an examination of potential cloud contamination in the Aqua MODIS aerosol product through the use of collocated CALIOP data.

As mentioned above, there is limited suitable ground-based infrastructure from which to supplement passive satellite measurements in the study region, and thus isolating the physical mechanisms (i.e., cloud contamination) responsible for ESOA is non-trivial. Therefore, active-based satellite profiling (e.g., lidar and/or radar) represents a complimentary and symbiotic means for interpreting particle layer presence and scattering, and thus enhanced column radiances in passive datasets (e.g., Chew et al. 2011). In this study, datasets collected with the NASA CALIOP, a multi-wavelength (0.532 and 1.064  $\mu\text{m}$ ) polarization-sensitive instrument flown within the NASA A-Train (Stephens et al. 2002), are used to investigate if unscreened cloud presence in the Aqua MODIS over-ocean aerosol product causes ESOA. Therefore, the following research questions are addressed: Is ESOA the result of unscreened cloudiness? Do active-profilers help screen the passive datasets more thoroughly in order to suppress ESOA? What types of clouds (i.e., ice or liquid water) are passing through MODIS screening protocols?

## CHAPTER II

### DATA AND METHODOLOGY

#### Ground-Based Observations

The first goal of this work is to consider MAN data relative to Aqua MODIS datasets to investigate if ESOA is evident from a ground-based perspective. Many studies have relied on AERONET datasets for validating passive satellite retrievals over the last decade (e.g., Kaufman et al. 2005; Shi et al. 2011; Sayer et al. 2012), as they are considered benchmarks for aerosol particle optical properties observed worldwide (e.g., Chin et al. 2002; Yu et al., 2003). AERONET is the parent network of MAN, and provides observations of aerosol properties over land through the use of sun photometers (Holben et al. 1998). However, over the Southern Oceans, the lack of land, and therefore the lack of possible AERONET coverage, leaves few remaining options for following such a well-established paradigm. MAN, however, despite providing only a few measurements in comparison to the wealth of data typically compiled from AERONET within comparatively sized domains, is practical for performing this task. Note that this is possible despite the majority of data points being collected in the summer hemispheric months, as opposed to the darker winter ones.

MAN AOD data are collected through ship-borne operations (at irregular intervals and locations) where hand-held Microtops II sun photometers measure the amount of energy transmitted to earth's surface in five spectral channels ranging from 0.340-1.020  $\mu\text{m}$ . To calculate AOD ( $\tau$ ) from these intensities, Beer's Law is utilized:

$$I = I_0 e^{-\tau}, \quad (1)$$

where  $I$  is intensity of solar radiation measured by the sun photometer and  $I_0$  is the intensity of solar radiation at the top of earth's atmosphere. The uncertainty of these observations is  $\pm 0.02$  (Smirnov et al. 2011). For consistency, as will be described with Aqua MODIS, AOD at  $0.550 \mu\text{m}$ , derived from the Level 2 MAN Spectral AOD product, are considered here. In the absence of a  $0.550 \mu\text{m}$  channel, however, this value is solved through interpolation from AOD measured at  $0.500$  and  $0.675 \mu\text{m}$  using an Angstrom relationship (e.g., Shi et al. 2011). For collocation and comparison, MAN data are required temporally to be within  $\pm 30$  min of a collocated Aqua MODIS retrieval and spatially within  $\pm 0.3^\circ$  latitude/longitude. If these criteria are not met, no MAN comparison is performed. To increase the sample size, the northerly extent of the Southern Oceans domain is shifted slightly to  $40^\circ$  S, with a temporal range of 2004 through 2011.

To supplement MAN observations, three years (2007-2009) of surface data from two AERONET instruments, Dunedin ( $45.9^\circ\text{S}$ ,  $170.5^\circ\text{E}$ ) and Crozet ( $46.4^\circ\text{S}$ ,  $51.9^\circ\text{E}$ ), are analyzed. AERONET AOD, like MAN AOD, is derived through the use of sun photometers and Beer's Law (Equation 1). The uncertainty of AERONET AOD measurements is about 0.01 to 0.015 (Holben et al. 1998). The Aqua MODIS collocation here is the same as performed for MAN, and AOD at  $0.550 \mu\text{m}$  is solved from AERONET data using the same interpolation method of available/reported channels.

### Passive Satellite Observations

Passive satellite remote sensors use electromagnetic energy provided by the sun or the Earth (Purkis and Klemas 2011). The coverage and field-of-view (FOV) of



passive satellites make them useful in studies with large domains, such as the Southern Oceans region. An example of a passive sensor that has observed ESOA is MODIS, a spectroradiometer onboard NASA's Aqua satellite with 36 spectral channels ranging from 0.41 to 15  $\mu\text{m}$  (Remer et al. 2005). The aerosol retrieval spans seven channels (0.47 to 2.13  $\mu\text{m}$ ), but this work investigates ESOA with only the over ocean 0.550  $\mu\text{m}$  aerosol retrieval, which has an uncertainty of  $0.03 \pm 0.05 \cdot \text{AOD}$  (Remer et al. 2005).

The MODIS ocean aerosol algorithm is a complicated process, requiring calibrated, geolocated reflectances of the surface, and involving cloud, sediment, and ocean glint masking procedures. The optical properties of aerosols are determined through a Look Up Table (LUT) process, consisting of three steps. First, a radiative transfer model is utilized for the computation of satellite radiances (which form the LUT) over each of the seven available wavelengths as functions of predetermined observations and aerosol models. For small mode aerosols, four models are used, while five are used for large mode aerosols. Next, the spectral radiances observed by the satellite are matched to the calculated radiance from the LUT until a minimum difference between the two is reached. Lastly, the aerosol model values from the second step are assumed to be first order solutions, and aerosol properties (such as AOD) are derived from the aerosol parameters of the aerosol models (Remer et al. 2005). While the theoretical basis for this algorithm has not changed since its implementation, some mechanics have been improved upon with successive "collections," or groups of MODIS data. As such, Collection 5.1, the most recent MODIS data available, is used.

For greater specificity, three years (2007-2009) of Aqua MODIS Level 2 aerosol product (MYD04\_L2) datasets are used in this analysis, and are reported at a 10x10 km

spatial resolution. The Effective Optical Depth Best Ocean (EODBO;  $0.550 \mu\text{m}$ ) and Cloud Fraction Ocean (CFO) parameters are considered (the latter being used since our domain is encapsulated almost solely by water at the surface). Note that the CFO represents the percentage of pixels excluded from retrieval processes, such as cloudy pixels and observations in glint regions (Zhang et al. 2005). The Quality Assurance Ocean (QAO) parameter is considered in order to constrain these two datasets to their highest potential quality, thus retrievals flagged as 1 (marginal), 2 (good), or 3 (very good) are included.

### Active Satellite Observations

Active remote sensors, such as Radio Detection And Ranging (RADAR) and Light Detection And Ranging (LIDAR), transmit energy through a pulse (Purkis and Klemas 2011). While the limitation of active remote sensors is their small spatial coverage, they provide useful vertical measurements of atmospheric properties. An example of an active remote sensor is CALIOP, the multi-wavelength ( $0.532$  and  $1.064 \mu\text{m}$ ) lidar associated with NASA's Cloud-Aerosol Lidar and Infrared Pathfinder Satellite Observations (CALIPSO) mission (Winker et al. 2012). CALIOP provides the measurements necessary to obtain the vertical structure of aerosols and clouds in the atmosphere, and its data are used extensively throughout this study of ESOA.

CALIPSO Level 2 data are separated into three products (CALIPSO Data Products Catalog 2006): layer products, profile products, and the vertical feature mask (VFM). Layer products contain layer-integrated or layer-averaged properties of the aerosol and cloud layers detected by CALIOP. For this study, daytime Version 3.01 Level 2 5 km Aerosol Layer (L2\_05kmALay) product datasets are used for QA purposes, and daytime

Version 3.01 Level 2 5km Cloud Layer (L2\_05kmCLay) product datasets are used for analysis of the vertical distribution of clouds.

There are also profile products, which contain the retrieved extinction and backscatter profiles within the aerosol and cloud layers detected by CALIOP. The work presented here uses daytime Version 3.01 Level 2 5 km Aerosol Profile (L2\_05kmAProf) product datasets for QA purposes and the computation of column AOD. CALIOP column AOD retrievals have an uncertainty of about  $\pm 13\%$ , relative to AERONET AOD observations (Schuster et al. 2012). The L2\_05kmAProf datasets are also employed during the collocation of CALIOP and Aqua MODIS AOD, the method for which is outlined in a later section of this text.

Finally, the VFM is a feature classification product that provides information on the location and type of aerosols and clouds within CALIOP retrievals (Winker et al. 2012). For this study, daytime Version 3.01 Level 2 Vertical Feature Mask (L2\_VFM) data are used for layer type discrimination (i.e., aerosol vs. cloud) and their column distributions, thus integrating the full range of CALIOP spatial averaging schemes applied for optimal layer detection and characterization (e.g., Vaughan et al. 2009). This feature classification is an important component of the methods employed to study ESOA, discussed in greater depth in a later section. The parameters of the VFM product used for this work, and those of the layer and profile products, are listed in Table 1.

Table 1. CALIPSO products and parameters utilized in this study.

<b>CALIPSO Product</b>	<b>Parameters Used</b>
Aerosol Layer	Integrated Attenuated Backscatter 532
Aerosol Profile	Profile UTC Time, Latitude, Longitude, Extinction Coefficient 532, Extinction QC 532, Extinction Coefficient Uncertainty 532, CAD Score, Atmospheric Volume Description
Cloud Layer	Layer Top Altitude, Layer Base Altitude, Layer Top Temperature, Layer Base Temperature
Vertical Feature Mask	Feature Classification Flags

#### Collocation Method and Collocated Data Subsets

For January 2007 through December 2009, Aqua MODIS datasets, consistent with those described in a previous section, are collocated with two subsets of L2\_05kmAProf product datasets: one where cloud identification is available (i.e., successful cloud algorithm retrievals), and another where aerosol particle profiling is available. This collocation is based on spatial proximity. The starting and ending times of each L2\_05kmAProf daytime file are first considered and 5 minutes are subtracted from the starting time and added to the ending time to temporally match with the concurrent Aqua MODIS retrieval, again propagating within the A-Train in sequence ahead of CALIOP. Those matching Aqua MODIS composites found are then analyzed. Spatially, CALIOP and Aqua MODIS AOD observations are considered collocated when the center of an Aqua MODIS 10 km x 10 km retrieval is identified within 8 km of the temporal midpoint for a 5-km L2\_05kmAProf profile. If this criterion is not met, no collocation is performed. This is similar to the collocation methodology of Kittaka et al. (2011), though their method is predicated on a 10 km separation between coincident points. Figure 2 illustrates the collocation process used in this study.

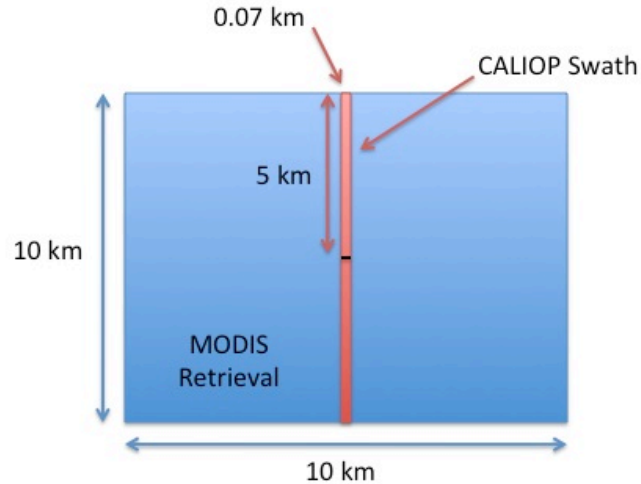


Figure 2. The spatial collocation of CALIOP and Aqua MODIS datasets. In this example, there are two 5-km CALIOP segments for one 10x10 km MODIS retrieval.

Also, note that the collocation process presented here considers only nadir viewing AOD measurements. However, the MODIS retrieval accuracy may also be a function of viewing geometry such as viewing zenith angle (e.g., Hyer et al. 2011; Shi et al. 2011), but the effects of this on ESOA fall outside the focus of this work.

For each collocation, an initial Aqua MODIS/CALIOP subset is generated for those data points where both valid Aqua MODIS EODBO and QAO values are reported in tandem with an equally valid L2\_VFM record, and where fifteen L2\_VFM 0.333 km resolution profiles are found that correspond with the 5 km L2\_05kmAProf profile. For this first subset, these data are considered irrespective of whether or not a valid aerosol profile retrieval is solved, therefore maximizing the amount of Aqua MODIS data available for study relative to CALIOP L2\_VFM estimates of cloudiness. This subset is heretofore referred to as CALIOP\_Cloud. A second subset, CALIOP\_Aerosol, is constructed for cases in which a valid L2\_05kmAProf retrieval is available, and from which a CALIOP-iterated solution for column 0.532  $\mu\text{m}$  AOD is subsequently derived

(Omar et al. 2009; Young and Vaughan, 2009). To derive CALIOP column AOD ( $\tau$ ), the Extinction Coefficient 532 ( $\beta$ ) is integrated throughout the entire atmospheric profile. It is computed using

$$\tau = \int_0^z \beta dz, \quad (2)$$

where  $z$  represents altitude. Note that profiles where AOD is solved as zero after CALIOP QA screening are considered invalid and removed from the CALIOP\_Aerosol subset.

Before deriving AOD, however, L2\_05kmAProf extinction coefficient profiles are subject to supplemental QA screening before a solution is reached. The data screening procedures for this study are similar to the ones implemented by Kittaka et al. (2011) and Campbell et al. (2012). An extinction coefficient is considered quality assured and included in a column AOD calculation when all of the following criteria are satisfied:

1.  $0 \text{ km}^{-1} \leq \text{Extinction Coefficient 532} \leq 1.25 \text{ km}^{-1}$ .
2. Extinction QC 532 is equal to 0, 1, 2, 16 or 18,
3.  $-20 \geq \text{CAD Score} \geq -100$ ,
4. Extinction Coefficient Uncertainty 532  $\leq 10 \text{ km}^{-1}$ ,
5. Atmospheric Volume Description (bits 1–3) is equal to 3,
6. Atmospheric Volume Description (bits 10–12) is not equal to 0, and
7. Integrated Attenuated Backscatter 532  $\leq 0.01 \text{ sr}^{-1}$ .

It is noted that, because L2\_05kmAProf files include data at 60 m vertical resolution, measurements below 8.2 km are two-bin averages of raw 30 m resolution data. As such, the QA screening process implemented in this study requires both bins of the Extinction

QC 532, CAD Score, and Atmospheric Volume Description parameters to satisfy the respective criteria.

Values of Extinction Coefficient 532 between  $0 \text{ km}^{-1}$  and  $1.25 \text{ km}^{-1}$  are considered valid, as documented in the CALIPSO Data Products Catalog (NASA, 2011). The Extinction QC 532 parameter is a quality control flag, used to keep only the most reliable retrievals and reject all others (Campbell et al. 2012). The CAD Score is a measure of the confidence of the classification of a layer as aerosol or cloud within a bin. Negative values of CAD Score indicate the presence of aerosol (Campbell et al. 2012). Bins with Extinction Coefficient Uncertainty 532 greater than  $10 \text{ km}^{-1}$  signify unrepresentative values, and thus are removed from the analysis (Campbell et al. 2012). Bits 1-3 of the Atmospheric Volume Description parameter describe the type of scattering target identified by CALIOP. A value of '3' signifies the presence of aerosol particles. Furthermore, bits 10-12 of this parameter indicate the type of aerosol detected. A value of '0' is given for "not determined" instances, and thus is not considered QA (Campbell et al. 2012). Lastly, some aerosol layers may have extremely large layer-integrated attenuated backscatter values, which have been attributed to overcorrection of the attenuation of overlying layers (Kittaka et al. 2011). Thus, profiles composed of aerosol layers with integrated attenuated backscatter greater than  $0.01 \text{ sr}^{-1}$  are removed.

For simplicity, this narrative considers the respective  $0.550 \text{ }\mu\text{m}$  Aqua MODIS and  $0.532 \text{ }\mu\text{m}$  CALIOP AOD retrievals below without specifically referencing the wavelengths any further. It is further acknowledged that a slight difference when comparing AOD at these two wavelengths is to be expected, and estimated at 3% considering an Angstrom exponent relationship of 1.0 (e.g., Kitakka et al. 2011). Broad-

scale analyses described below reflect a domain bounded from 60° S to 60° N, as a function of significant collocated sample size and context relative to the Southern Oceans. For brevity, however, these samples are referred to as ‘global’.

For both subsets, cloud layers identified within an L2\_05kmAProf average, and reported in the L2\_VFM product, are designated as either:

1. Cirrus - Cirrus clouds present only
2. Other - Clouds present, but not distinguished as cirrus
3. Both - Both Cirrus and Other are present
4. SF (Stratospheric Feature) - Depicting the presence of polar stratospheric clouds or stratospheric aerosols
5. Clear - The column contains no cloud.

Each layer classified as Other or Both is broken into seven possible feature subcategories, designated within L2\_VFM. In the event that multiple sub-classifications occur within a single 5-km segment, the layer is assessed based on what feature is most prevalent relative to the number of bins classified in a single 0.333 km along-track profile (i.e., physical depth) multiplied by the number of lowest-level profiles (maximum of 15) in which it is deemed present (i.e., temporal persistence). To help illustrate this process, the horizontal and vertical resolutions of a 5-km L2\_VFM segment are shown in Fig. 3.



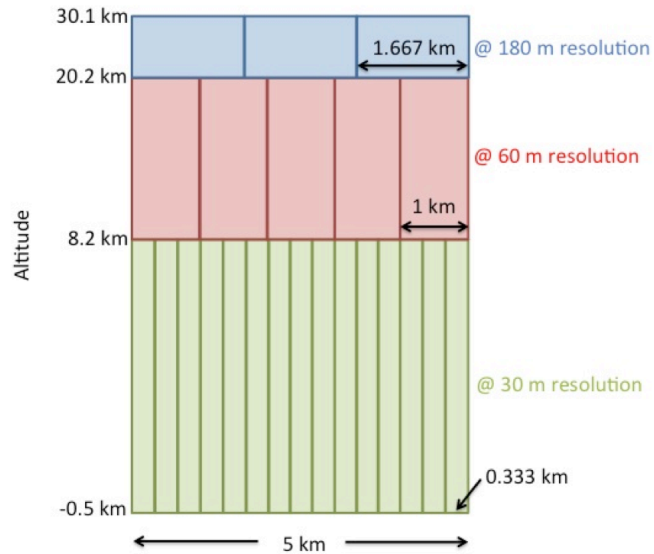


Figure 3. The horizontal and vertical resolutions of a 5-km CALIOP L2\_VFM file (duplicated from the CALIPSO Quality Statements webpage, [http://eosweb.larc.nasa.gov/PRODOCS/calipso/Quality\\_Summaries/CALIOP\\_L2VFMProducts\\_3.01.html](http://eosweb.larc.nasa.gov/PRODOCS/calipso/Quality_Summaries/CALIOP_L2VFMProducts_3.01.html), retrieved on December 5, 2012).

The possible cloud subcategories classified by the VFM are “low overcast, transparent” (LOT), “low overcast, opaque”, “transition stratocumulus” (TS), “low, broken cumulus” (LBC), “altocumulus (transparent)” (AT), “altostratus (opaque)”, and “deep convective (opaque)” (abbreviations given for those subcategories most dominant in this analysis; Liu et al. 2005). Within the language applied by the L2\_VFM product, Other represents a proxy for liquid water cloud presence. This is an assumption, however, as the ice/water phase flag in the L2\_VFM product is not used. Therefore, Other clouds are not always necessarily of the liquid water phase. To limit the ambiguity in classifying a subcategory in the event that multiple types are present in equal depth and persistence, these few cases (less than 0.1%) are removed.

Also, polar stratospheric clouds (PSCs) are not specifically identified and classified in the CALIOP data (personal communication with Dr. Mark Vaughan 2012).

Instead, CALIOP data only provide a very basic 'stratospheric layer' classification that encompasses both PSCs (all types) and stratospheric aerosols. Also, such a category represents a very small percentage of the data analyzed in this study (less than 1.0%). Therefore, the same convention is followed and both stratospheric aerosols and clouds are labeled as Stratospheric Feature (SF). Lastly, low cloud flags (LBC, LOT, and TS) in the VFM datasets have exhibited questionable skill, and changes to this product are pending future data releases (personal communication with Dr. David Winker 2012). As a first-order estimate of cloud fraction, however, the data are applied here with this caveat implied in order to further cloud screen the data conservatively. As will be shown, this does not significantly influence the final result.

It is noted that, particularly with respect to cirrus clouds, the L2\_VFM file includes clouds detected at horizontal averaging intervals in excess of a 5 km L2\_05kmAProf file (i.e., 20 and 80 km spatial resolutions). It is recognized that cloud identification from the VFM, and used for screening MODIS and CALIOP AOD subsets in the series of analyses described, can result in some measure of representativeness bias due to these extended averaging intervals (Yorks et al. 2011). However, this serves to create the most conservative estimate of cloud presence possible from CALIOP relative to MODIS, which for the purposes of this study is believed an asset.

For each subset (CALIOP\_Cloud and CALIOP\_Aerosol), three sets of analyses are performed, and described in the following section, using the collocated Aqua MODIS CFO and CALIOP L2\_VFM datasets. The first represents Aqua MODIS AOD averages derived when  $CFO \leq 100$ , referred to as AM-100, which represents those EODBO AOD values where any cloud fraction (0.0 to 1.0) is allowed. Some past studies (e.g., Zhang et

al. 2005) have used a cloud fraction of 0.8 as an upper threshold, and thus an AM-80 (0.0 to 0.8 CFO) analysis is briefly shown later for comparison. However, this study utilizes cloud fractions of 0 and 1.0 as lower and upper limits in order to consider the maximum possible cloudiness. Second, an analysis is conducted when CFO = 0, or when MODIS algorithms identify no clouds present within the bounds of the collocated 10 km<sup>2</sup> retrieval, and thus representing cases where MODIS algorithms have been applied exclusively for cloud screening of the apparent scene. This case is referred to as AM-0. Third, the latter sample is reexamined using the CALIOP L2\_VFM product to eliminate any residual cloud-contaminated points identified with the lidar. This analysis is referred to as AM-CALIOP. Differences in mean AOD retrieved for each case, and in successive order of more thorough screening, are used to interpret the effects of cloudiness on Aqua MODIS AOD, identified both passively and actively, and consequently on ESOA.

The two data sets, CALIOP\_Cloud and CALIOP\_Aerosol, have been delineated since the former considers all collocated Aqua MODIS points possible with information on potential cloud coincidence characterized from the lidar, and the latter allows for consideration of CALIOP AOD in order to establish context for comparison with Aqua MODIS AOD as a function of successive cloud screening protocols. The criteria for each sample and the three corresponding analyses are summarized in Table 2.

Table 2. The criteria for each subset analysis and their respective products.

Analysis	Product Name	Criteria		
		CFO	CALIOP VFM	CALIOP AOD
<i>CALIOP_Cloud</i>	AM-100	0.0 – 1.0	Valid	-
	AM-0	0	Valid	-
	AM-CALIOP	0	Only clear; valid	-
<i>CALIOP_Aerosol</i>	AM-100	0.0 – 1.0	-	> 0
	AM-0	0	-	> 0
	AM-CALIOP	0	Only clear; valid	> 0

### The Spatial Representativeness Problem

If CALIOP cloud fraction is considered representative of that for a collocated MODIS 10 km x 10 km composite data point, the finite sampling width of the laser footprint (70 m across the track, 330 m along the track at the surface) correlates with some statistical probability that the lidar will actually detect clouds within the bounds of the MODIS retrieval. The requirement that MODIS and CALIOP midpoints be within 8 km of one another does not guarantee that either a given CALIOP 5-km segment coincides with or falls entirely within the bounds of the collocated MODIS observation. However, most collocated data points have two CALIOP 5-km segments associated with the same MODIS 10 km x 10 km composite. One CALIOP 5-km segment, given its surface footprint, translates to about 0.35 km<sup>2</sup> coverage compared with 100.0 km<sup>2</sup> area sample by MODIS. Thus, two 5-km CALIOP segments equal 0.7 km<sup>2</sup> coverage, rounded to a relative 1.0% (Fig. 2). In this unique case where the profiled area is extremely small relative to AM, the probability for detection of a broken cloud scene converges to that of the cloud fraction itself (otherwise, the solution would approach unity as the profiling swath approached that of the sampling area).

In general, the probability of CALIOP detection within a 10 km x 10 km MODIS retrieval (Kreyszig 2006) is calculated by taking 1.0 and subtracting the combination of cases for cloud detection outside the CALIOP overpass ( ${}_{99}C_{CF}$ ) divided by the combination of cases for all cloud detection ( ${}_{100}C_{CF}$ ). Both the numerator and denominator are computed as a function of a particular CALIOP cloud fraction (CF). It is noted that CALIOP cloud fraction is assumed to be representative of the cloud fraction of the MODIS retrieval. In equation form, the probability of CALIOP detection, assuming 1.0% CALIOP coverage, is

$$1.0 - ({}_{99}C_{CF} \div {}_{100}C_{CF}). \quad (3)$$

For TS clouds and a mean CALIOP cloud fraction of about 0.7, the probability of CALIOP detection is

$$1.0 - ({}_{99}C_{70} \div {}_{100}C_{70}) = \frac{\binom{99!}{(70! \cdot 29!)}}{\binom{100!}{(70! \cdot 30!)}} = 0.7. \quad (4)$$

For LBC clouds, this same calculation, given a mean CALIOP cloud fraction of about 0.2, results in a probability of detection of

$$1.0 - ({}_{99}C_{20} \div {}_{100}C_{20}) = \frac{\binom{99!}{(20! \cdot 79!)}}{\binom{100!}{(20! \cdot 80!)}} = 0.2. \quad (5)$$

Therefore, CALIOP cloud screening of the AM datasets is incomplete relative to the statistical probability that the lidar profile actually coincides with a cloud. As such, the goal here is to correct for this incomplete cloud screening through a conservative estimate of possible cloud contamination. TS and LBC are the only clouds reported in the L2\_VFM with cloud fractions less than 1.0, and thus their relative incidence rates identified in the AM-0 residual are undersampled. The amount of this undersampling is

represented by an undersampling factor, computed by inverting the solutions of Equations 4 and 5 and then subtracting 1.0. For LBC clouds this is

$$\frac{1}{0.2} = 5 - 1 = 4. \quad (6)$$

For TS clouds this is

$$\frac{1}{0.7} = 1.428 - 1 = 0.428. \quad (7)$$

Note that LOT clouds are not impacted here, since cloud fraction is 1.0, corresponding with a 100% chance of detection and screening. This implies the undersampling factor for this case is 0, given by

$$\frac{1}{1} = 1 - 1 = 0. \quad (8)$$

Therefore, AM-CALIOP AM AOD can be renormalized based on relative incidence rates and mean respective AOD at 1° meridional resolution to compensate for approximate TS and LBC undersampling.

The renormalized AM-CALIOP AM AOD global profile is computed as

$$New\ AOD = \frac{(Z - HX - JY)}{K}, \quad (9)$$

where  $Z$  represents the zonal mean of AM-CALIOP AM AOD.  $H$  and  $J$  are the approximated zonal percentages of undersampled LBC and TS points, respectively, computed using the number of LBC and TS points from the AM-0 analysis and the undersampling factors shown above.  $X$  and  $Y$  are the average values of AM AOD for LBC and TS for the entire Southern Oceans region. As such, these values are presumed constant for each 1° zonal band due to small sample sizes in 1° meridional bands alone.  $K$  is the zonal percentage of uncontaminated points in the AM-CALIOP AM sample, computed using

$$K = \frac{(F-(D+E))}{F} = 1 - H - J, \quad (10)$$

where F is the total number of points in the AM-CALIOP sample (computed zonally), while D and E are the approximated zonal number of undersampled LBC and TS points from the AM-0 analysis, respectively, computed using the undersampling factors described earlier. For a sensitivity analysis, a similar method is applied to find New AOD 2. This time, however, the values of X and Y are found using zonal averages of AM AOD for LBC and TS, and these values vary with latitude.

## CHAPTER III

### RESULTS AND DISCUSSION

#### Analysis of Ground-Based AOD Observations

The initial analysis of this thesis investigates ESOA using ground-based AOD observations from MAN and AERONET relative to Aqua MODIS datasets. First, nearly two hundred MAN/Aqua MODIS collocations are performed for the 2004-2011 period. A comparison of AOD reported by the two sensors is shown in Fig. 4.

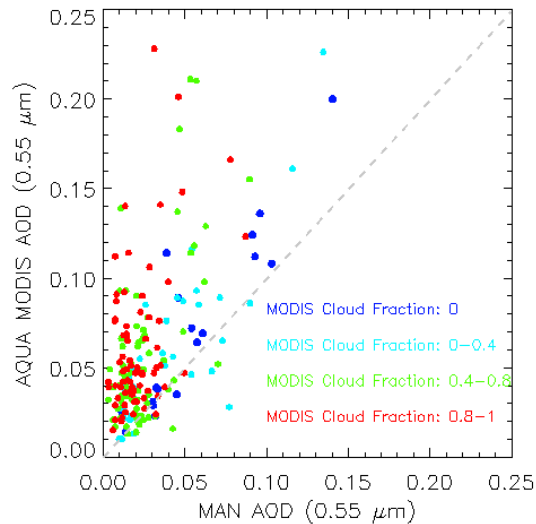


Figure 4. Scatterplot of Maritime Aerosol Network (MAN) AOD vs. Aqua MODIS (AM) AOD for 2004 to 2011 for latitudes south of 40°S. The one-to-one line is in gray, and the data points are colored based on AM cloud fraction.

Consistent with Smirnov et al. (2011), the average difference between AM and MAN AOD is about 0.03. Further, regardless of cloud fraction reported, AM AOD is usually higher than MAN AOD. Greater differences between the two sensors are generally found for larger cloud fractions, indicating the impact of cloud contamination.



MAN cloud screening is based on AERONET protocols, for which some incidence of sample bias due to misidentified cloudiness is possible. This is particularly evident with optically thin and spatially persistent cirrus cloud presence (Chew et al. 2011), for which 0.03 compares well with estimates of effective optical depth thresholds of sub-visual cloud occurrence (Sassen and Cho, 1992). It should be noted, however, that a seasonal bias exists, as MAN observations taken during Southern Hemisphere winter are scarcer than those taken during the Southern Hemisphere summer months.

For the AERONET/Aqua MODIS analysis, a comparison of the 89 (Dunedin) and 37 (Crozet) available data points are shown in Figs. 5a and b, respectively, for each site.

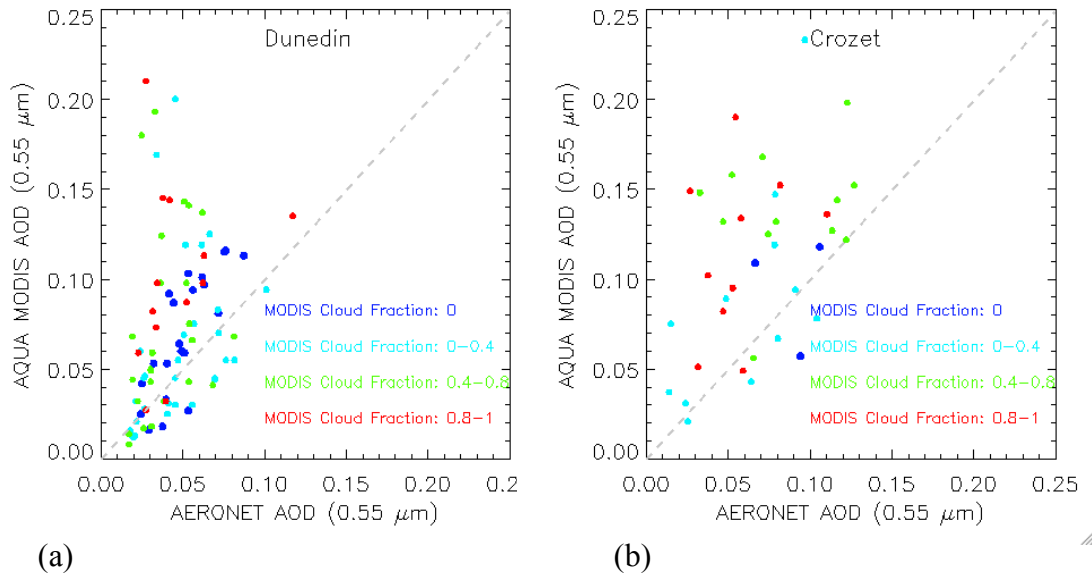


Figure 5. Scatterplots of Aerosol Robotic Network (AERONET) AOD vs. Aqua MODIS (AM) AOD for 2007 to 2009 at (a) Dunedin and (b) Crozet. The one-to-one lines are in gray, and the data points are colored based on AM cloud fraction.

Similar to the findings in the MAN comparison, AM AOD is uniformly larger than the AERONET estimates, and again regardless of cloud fraction. While the highest AM AOD values generally correspond to larger cloud fractions, this pattern is not as

pronounced as found versus MAN in Fig. 4. Table 3 shows mean values of AM, MAN, and AERONET 0.550  $\mu\text{m}$  AOD for all points from each of the collocated samples described, as well as only those with a reported AM cloud fraction of 0%.

Table 3. Mean values of Aqua MODIS, MAN, Crozet, and Dunedin AOD for all points in each dataset, as well as only those with a MODIS cloud fraction of 0%.

Analysis	MAN		Dunedin		Crozet		Aqua MODIS	
	All	0% CFO	All	0% CFO	All	0% CFO	All	0% CFO
MAN/Aqua MODIS	0.029	0.056	-	-	-	-	0.062	0.073
Dunedin/Aqua MODIS	-	-	0.046	0.051	-	-	0.072	0.069
Crozet/Aqua MODIS	-	-	-	-	0.070	0.089	0.111	0.095

Note that the AOD differences reported here are consistent with Jaegle et al. (2011), as they showed seasonally averaged AM AOD from 2005-2008 are higher than AERONET at Dunedin and Crozet. For this study, nearly 2400 MAN data points from 40°S to 70°S are used to construct Fig. 1h. Despite the seasonal sampling bias from MAN data, statistically, if ESOA does exist over cloud free skies, the ESOA signal should be observed from the multi-year analysis of MAN or AERONET data (e.g. Figs. 1h and 4). However, the ESOA signal is not evident from the multi-year ground based observations from MAN or AERONET data. Thus, statistically, the ESOA signal reported in the AM measurements cannot be confirmed by the available ground-based and ship-borne measurements over cloud free skies.

#### CALIOP/Aqua MODIS Collocated Analyses

As suggested in the previous section, under cloud free skies, the ESOA feature is not observed from ground-based observations using 8 years of MAN and 3 years of AERONET data. Therefore, questions arise, such as (1) is ESOA caused by cloud contamination? and (2) do passive sensors, like MODIS, observe ESOA under cloud free skies? In this section, the above two questions are addressed by using aerosol and

cloud products from CALIOP, as it exhibits much finer spatial and vertical resolutions (compared with MODIS) and thus has a better chance of detecting sub-pixel sized clouds and cirrus. Both of these are sources of contamination for the MODIS aerosol products (e.g. Zhang et al. 2005). The following discussion investigates the presence of ESOA in Aqua MODIS datasets for the CALIOP\_Cloud and CALIOP\_Aerosol analyses. Total data points for each sample and the three additional analyses (AM-100, AM-0, AM-CALIOP), along with their definitions and three-year mean Southern Oceans AOD values, are given in Table 4.

Table 4. For the CALIOP\_Cloud and CALIOP\_Aerosol analyses, each subset is described (AM-100, AM-0, and AM-CALIOP), and corresponding data point samples and mean Southern Oceans AOD are reported for the 2007-2009 time period of this study.

Analysis	Product Name	Criteria			Data Counts		Mean Southern Oceans AOD	
		CFO	CALIOP VFM	CALIOP AOD	Global Oceans	Southern Oceans	Aqua MODIS	CALIOP
<i>CALIOP_Cloud</i>	AM-100	0.0 – 1.0	Valid	-	9,835,710	779,337	0.158	0.086
	AM-0	0	Valid	-	1,978,417	166,313	0.107	0.066
	AM-CALIOP	0	Only clear; valid	-	1,656,337	141,416	0.101	0.065
<i>CALIOP_Aerosol</i>	AM-100	0.0 – 1.0	-	> 0	8,007,967	584,851	0.143	0.075
	AM-0	0	-	> 0	1,578,941	134,074	0.115	0.062
	AM-CALIOP	0	Only clear; valid	> 0	1,331,613	115,022	0.110	0.061

#### *CALIOP\_Cloud Subset Analysis*

Shown in Fig. 6 are global distributions of three-year (2007-2009) averaged AM AOD derived from the AM-100 analysis conducted for the CALIOP\_Cloud subset. The collocated AM and CALIOP data are binned into 1° by 1° grid bins. Corresponding bin-resolved sample sizes are depicted for this analysis in Fig. 6b.

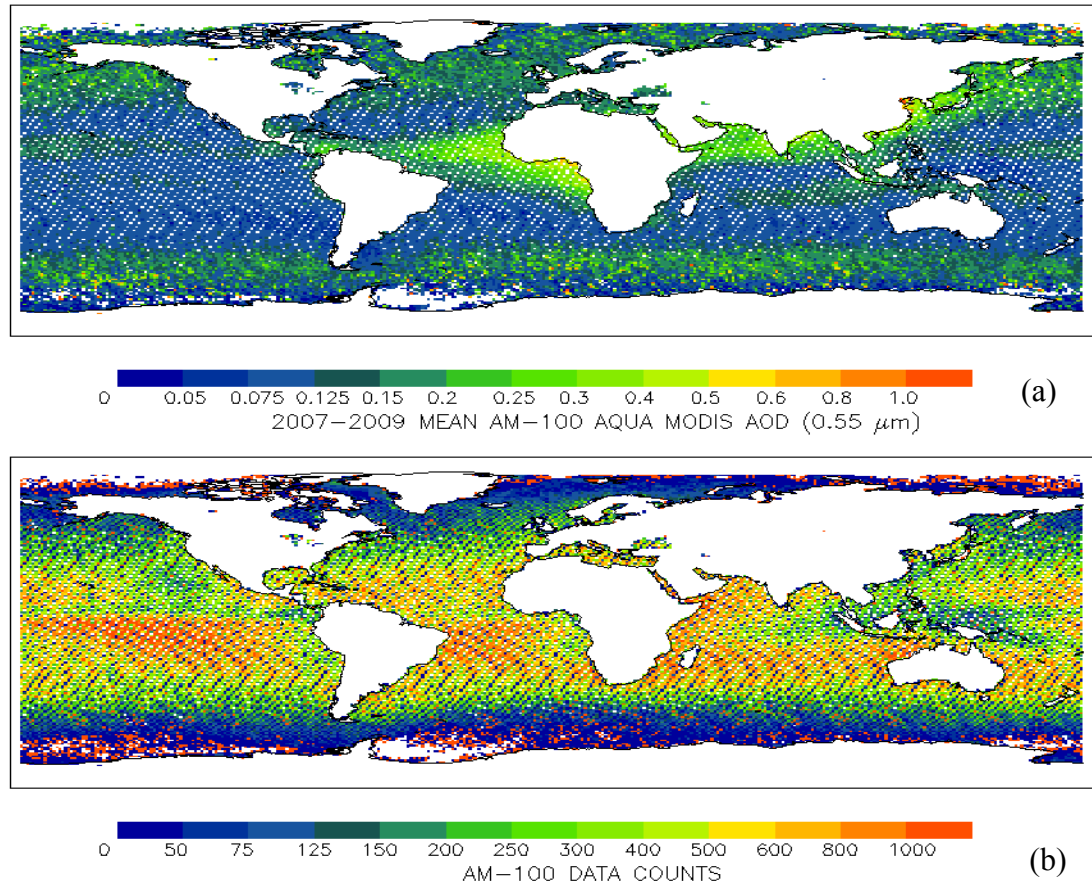


Figure 6. From 2007-2009, (a) AM-100 Aqua MODIS Collection 5.1 global mean AOD from over-ocean ‘marginal’, ‘good’, and ‘very good’ datasets and (b) their respective data counts, both displayed at  $1.0^\circ \times 1.0^\circ$  resolution.

With no restriction on AM cloud fraction in these data, bands and specific regions of relatively high AOD are observed over both the high latitudes of the Northern Hemisphere and in the Southern Hemisphere as a result of ESOA. Despite polar-orbiting ground tracks, for which more samples in the higher latitudes are expected from each hemisphere, most of the area in these two regions exhibit the lowest numbers of observations per grid box. Instead, high observation densities are located in the latitude bands just south of the Equator, as high latitudes experience winter seasons with much reduced data availability.

Figure 7a features corresponding global AOD distributions for the AM-0 case, which includes the cloud-free restriction based on AM algorithms. Shown in Fig. 7b is the corresponding AM-CALIOP analysis, with supplemental cloud screening applied to the AM-0 data using the CALIOP L2\_VFM product.

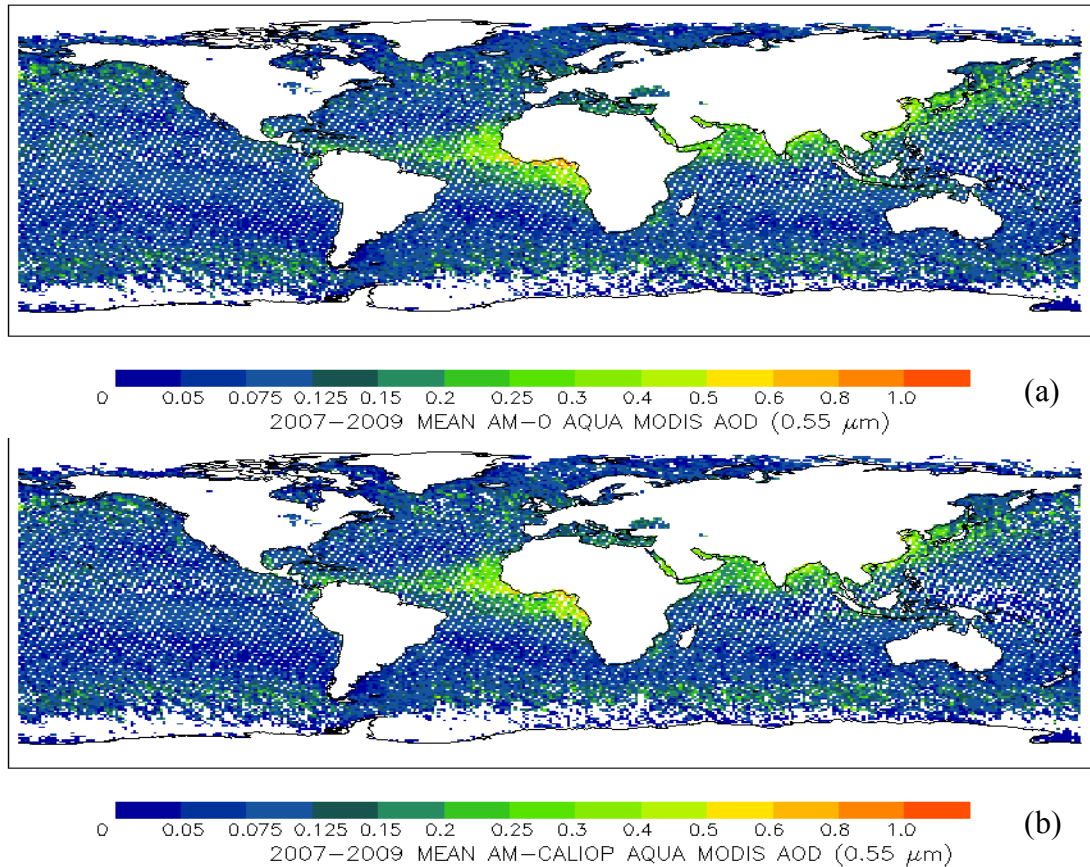


Figure 7. From 2007-2009, (a) AM-0 and (b) AM-CALIOP Aqua MODIS Collection 5.1 global mean AOD from over-ocean 'marginal', 'good', and 'very good' datasets, displayed at 1.0° x 1.0° resolution.

While high AOD values over the Equatorial regions are still present in the AM-0 composite, reduced AOD are found over the Northern Hemisphere high-latitudes and the Southern Oceans. However, despite active cloud detection conducted using the lidar for

screening any residual cloudiness missed by MODIS, significant AOD differences are not readily apparent in the latter plot (Fig. 7b).

These results are quantitatively depicted in Fig. 8, which includes the corresponding zonal AOD averages at 1° meridional resolution between 60° S and 60° N as derived for each of the three analyses, in addition to the AM-80 analysis (for comparison). While the Southern Oceans region extends to 65° S, the domain of Fig. 8 (along with Figs. 9, 13, and 17) is plotted to 60° S due to a limited amount of available data further south.

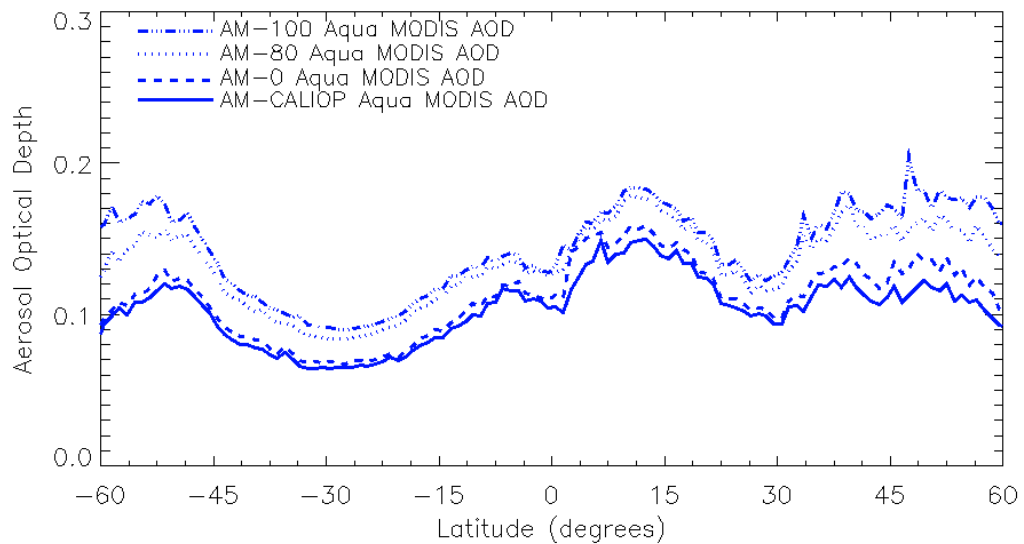


Figure 8. Three-year (2007-2009) global zonal mean of AM-100, AM-80, AM-0, and AM-CALIOP Aqua MODIS Collection 5.1 AOD datasets represented spatially in Figs. 6 and 7.

Significant change is observed between the AM-100 and AM-0 analyses, including a nearly 50% AOD reduction over the Southern Oceans that represents one of the highest such residuals apparent. Also, a slight decrease in AOD is observed between the AM-100 and AM-80 analyses. Some further reduction occurs between AM-0 and AM-

CALIOP, though magnitudes are generally lower than 10%, and the Southern Oceans region experiences the lowest relative change observed globally.

The data are reassessed and re-depicted in Fig. 9, where the corresponding zonal mean of CALIOP L2\_VFM classification percentage between 60° S and 60° N, for Clear, Cirrus, Other, Both, and SF are shown corresponding with the AM-100 (solid) and AM-0 (dashed) analyses.

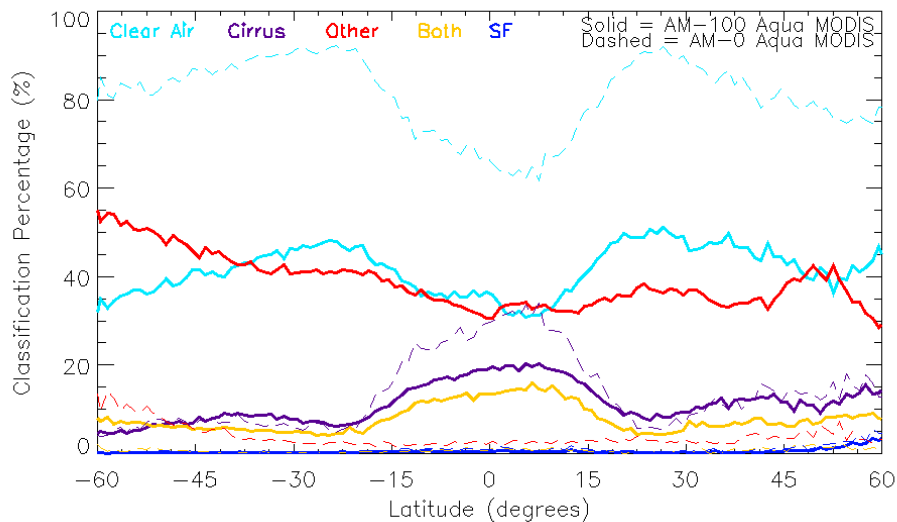


Figure 9. Three-year (2007-2009) global zonal mean of CALIOP VFM classification percentages from the AM-100 and AM-0 CALIOP\_Cloud analyses.

According to the L2\_VFM product, zonal mean collocated AM-100 samples correspond with Clear at a rate roughly 40% of the time globally. Cirrus occurrence is found at maxima in the tropics, near 20%, and approaches 5-15% nearing the poles. Cases of Other vary greatly over the global domain, between 30 and 60%. They are highest over the Southern Oceans. Incidence rates for Both are lower than that of Cirrus, except again over the Southern Oceans. SF is mostly negligible. Notably, however, over the Southern

Oceans domain, and unlike any other region, cases of Other are sampled more frequently than those of Clear.

When MODIS cloud screening is considered alone, cases of Other and Both drop significantly. The relative occurrence of Cirrus cases actually exceeds that found in the AM-100 sample in the tropics, in spite of the larger overall increase in Clear cases (> 60%). MODIS cloud screening shows no response to coincident cirrus cloud presence, identified with CALIOP, as do liquid water-phase clouds (e.g., Ackerman et al. 2008). In the AM-0 sample, Cirrus is identified more than Other north of 50° S. Over the Southern Oceans, clear air is the dominant scenario identified for this residual sample, with Other being second most frequent.

The AM-0 sample, with MODIS cloud fraction set to zero, should be completely cloud-cleared and all cases should be classified as Clear by the CALIOP L2\_VFM product. However, Fig. 9 shows relative residual cloudiness exists in the AM-0 sample. Relative classification percentages and total percentage of residual cloudiness relative to the L2\_VFM product identified in the AM-0 sample are shown for each zonal mean in Fig. 10.



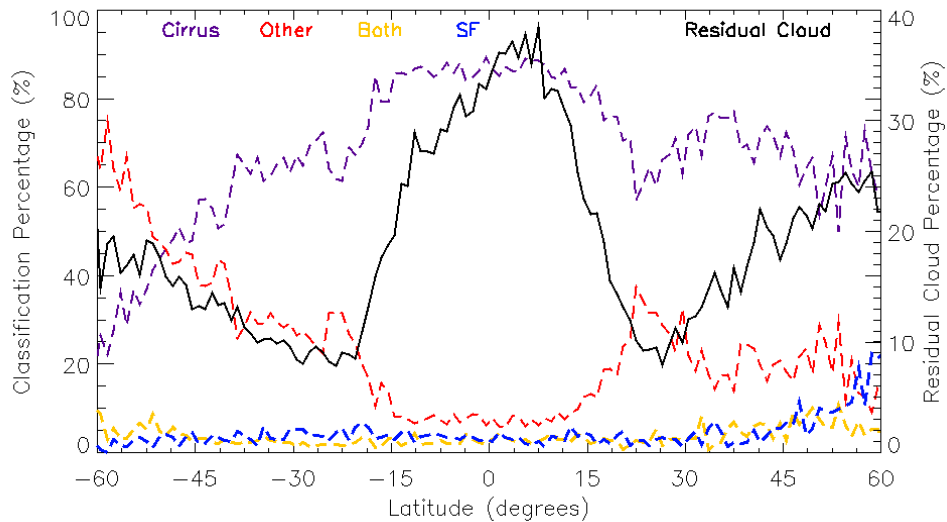


Figure 10. Three-year (2007-2009) global zonal mean of percentage of residual cloud plotted with the relative percentages of particular type of residual cloud in the AM-0 sample.

Residual cloudiness is apparent within 10-40% of the AM-0 sample globally, highest in the tropics due mostly to cirrus clouds, and lowest at  $\sim 20^\circ$  S and  $25^\circ$  N. Frequencies of residual cloudiness increase moving poleward (south and north, respectively) from the minima. As described above, over the Southern Hemisphere it is cases of Other that are most frequent, whereas in the north cirrus clouds remain the greater contributor. Over the Southern Oceans, however, liquid water phase clouds occur within the residual for between roughly 40 and 80% of the sample. This scenario is unique globally, and plausibly reflects the dominance of ocean coverage along this band, and possibly marine-type cloudiness (investigated below).

Sample sizes for Clear, Cirrus, Other, and Both are next investigated as a function of AM AOD. The AM-100 and AM-0 subsets are segregated into four corresponding AM

AOD bins: < 0.1, 0.1 to 0.2, 0.2 to 0.3, and > 0.3. Figure 11 first details classification percentages evaluated globally, for broader context.

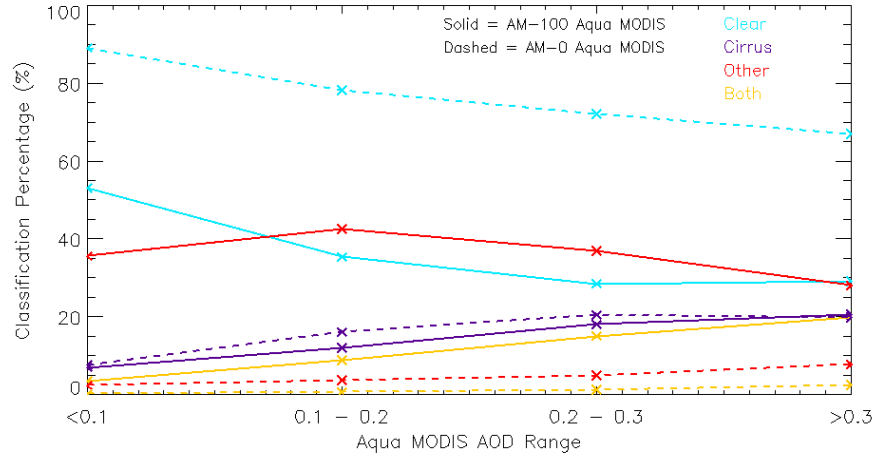


Figure 11. Three-year (2007-2009) CALIOP VFM classification percentages as a function of AM AOD from AM-100 and AM-0 CALIOP\_Cloud analyses for the globe.

For AM AOD > 0.3, the AM-100 sample contains a larger presence of Other than Cirrus. The opposite is true, however, for the AM-0 analysis. Consistent with Fig. 9, through the use of MODIS cloud screening, cloud contamination from Both and Other cases are much reduced, yet the percentage of Cirrus remains mostly the same. This suggests the cloud screening process used by MODIS developers in their aerosol retrievals is less effective in identifying and eliminating cirrus relative to liquid water clouds.

Focusing next on the Southern Oceans domain alone (Fig. 12), Other is the most prevalent non-Clear classification for both the AM-100 and AM-0 subsets for AM AOD greater than 0.3, but with a much reduced percentage in the AM-0 case.

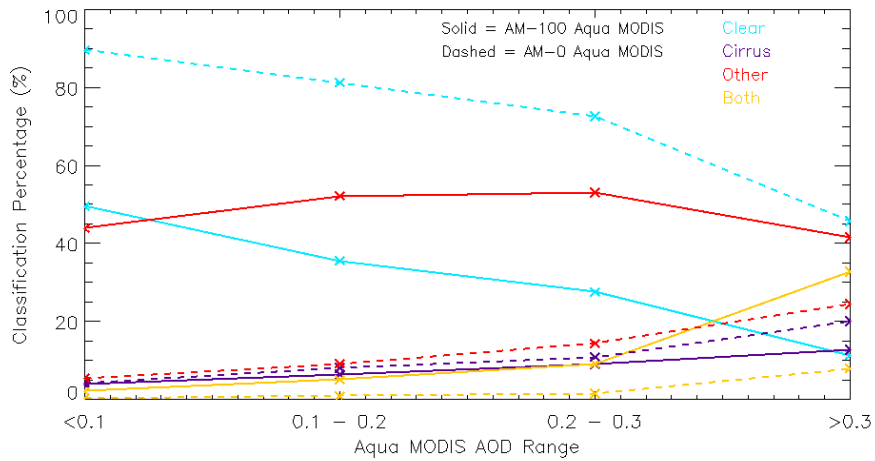


Figure 12. Three-year (2007-2009) CALIOP VFM classification percentages as a function of AM AOD from the AM-100 and AM-0 CALIOP\_Cloud analyses for the Southern Oceans region.

Considering the number of cases for the Other classification is larger than the Cirrus and Both classifications in the Southern Oceans region for the AM-100 and AM-0 subsets, the cloud sub-classifications of the Other category (Fig. 13) are now examined.

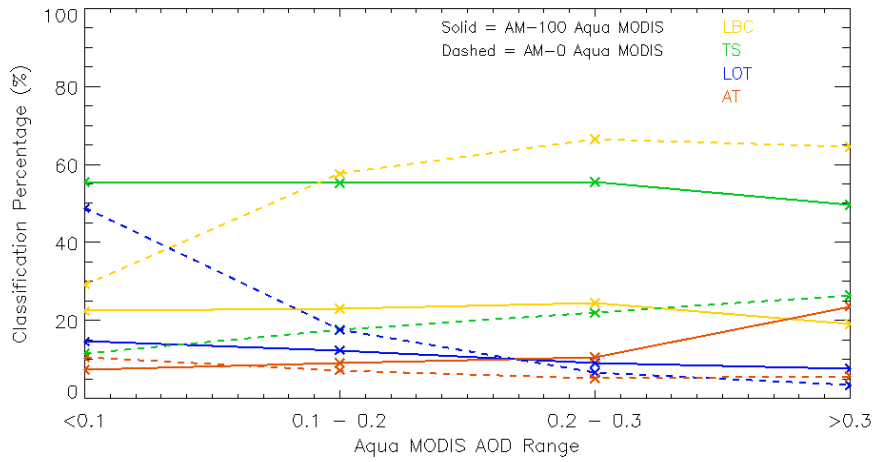


Figure 13. Three-year (2007-2009) relative CALIOP sub-classification percentages of the "Other" classification (shown in Fig. 12) as a function of AM AOD.

For the AM-100 analysis, TS clouds exhibit the largest presence, while the AM-0 analysis reveals LBC is the main cloud sub-classification. As such, TS and LBC likely cause the greatest cloud contamination of AM AOD retrievals over the Southern Oceans.

In Fig. 14, the vertical frequency distributions for cloud top height, in 1 km averaged bins (Fig. 14a), and cloud top temperature, in 5° C bins (Fig. 14b), are shown from the Southern Oceans domain for clouds identified with the L2\_VFM in both the AM-100 and AM-0 samples. The latter case represents the residual cloud sample described above in Fig. 10, whereas the former is from the raw MODIS aerosol product.

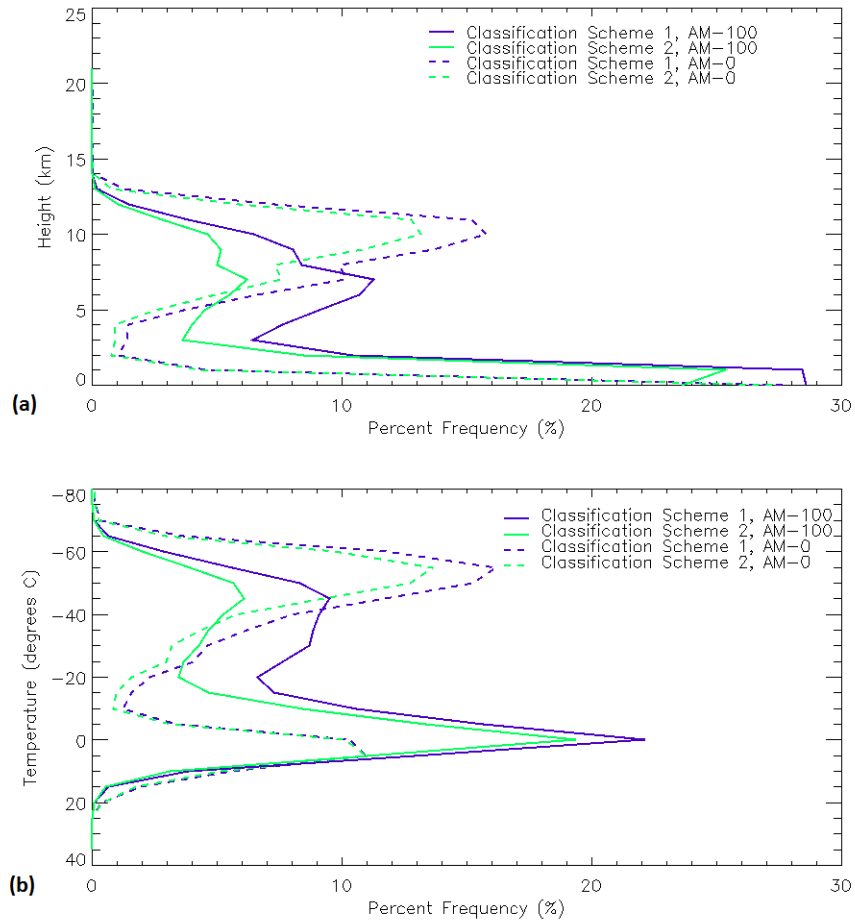


Figure 14. Vertical distribution of features classified by CALIOP VFM from the AM-100 and AM-0 CALIOP\_Cloud analyses as a function of (a) height and (b) temperature using two classification schemes. See the text for the differences between the two schemes.

For each sample, two sets of frequencies are computed. For Classification Scheme 1, frequencies are derived for all clouds, thus accounting for cases where multiple cloud layers are present and nominally exceeding 100%. Classification Scheme 2 distinguishes multi-layer cases by identifying only the one exhibiting the greatest temporal and spatial depth, and thus summing to 100% integrated frequency. Note that in Fig. 14a, the vertical axis extends past 20 km above mean sea level (MSL) from SF presence.

The AM-100 distribution is seen to be bimodal, with the dominant mode centered at an altitude of  $\sim 1$  km, corresponding to cloud top temperatures warmer than  $-10^{\circ}$  C, as shown in Fig. 14. Colder/higher cloudiness is more broadly distributed, though frequencies do increase slightly with altitude. From the AM-0 residual, however, distinct modes in cloud top height frequency are apparent near 10 km above MSL and again below 1 km MSL, corresponding with cloud top temperatures centered near  $-50^{\circ}$  C and again above  $-10^{\circ}$  C, respectively. The former represents cirrus cloud presence, since this mean cloud top height temperature is well below  $-38^{\circ}$  C, or the temperature for homogeneous freezing of liquid water that is believed the predominant mechanism responsible for cirrus cloud presence (e.g., Sassen and Campbell, 2001). The latter mode is representative of liquid water phase cloudiness nearing the ocean surface and presumably embedded within the marine boundary layer.

Frey et al. (2008) describe updates to the MODIS Collection 5 algorithm designed for better identifying stratocumulus clouds of limited horizontal extent, since cloud top radiances from these relatively warm clouds are difficult to differentiate from that of the background sea surface alone. That this lower/warmer mode represents the highest frequency for cloud presence identified in the Southern Oceans is potentially significant with respect to ESOA occurrence. It is further interesting to note that there is no relatively significant mode for mid-level cloudiness with the AM-0 sample relative to AM-100 observed (e.g., altocumulus; Gedzelman, 1988), since these clouds can also be spatially fractured, physically thin, and seemingly a candidate for misidentification from passive sensors. This topic is reexamined below.

### *CALIOP\_Aerosol Subset Analysis*

Next considered is the CALIOP\_Aerosol analysis, which again is constructed for cases in which a valid L2\_05kmAProf retrieval is available, and from which a CALIOP-iterated solution for column  $0.532 \mu\text{m}$  AOD is derived. Fig. 15a-c depicts global distributions of mean  $1^\circ \times 1^\circ$  CALIOP AOD derived for the AM-100, AM-0 and AM-CALIOP samples from the CALIOP\_Aerosol analysis. Sample sizes are provided in Table 4.

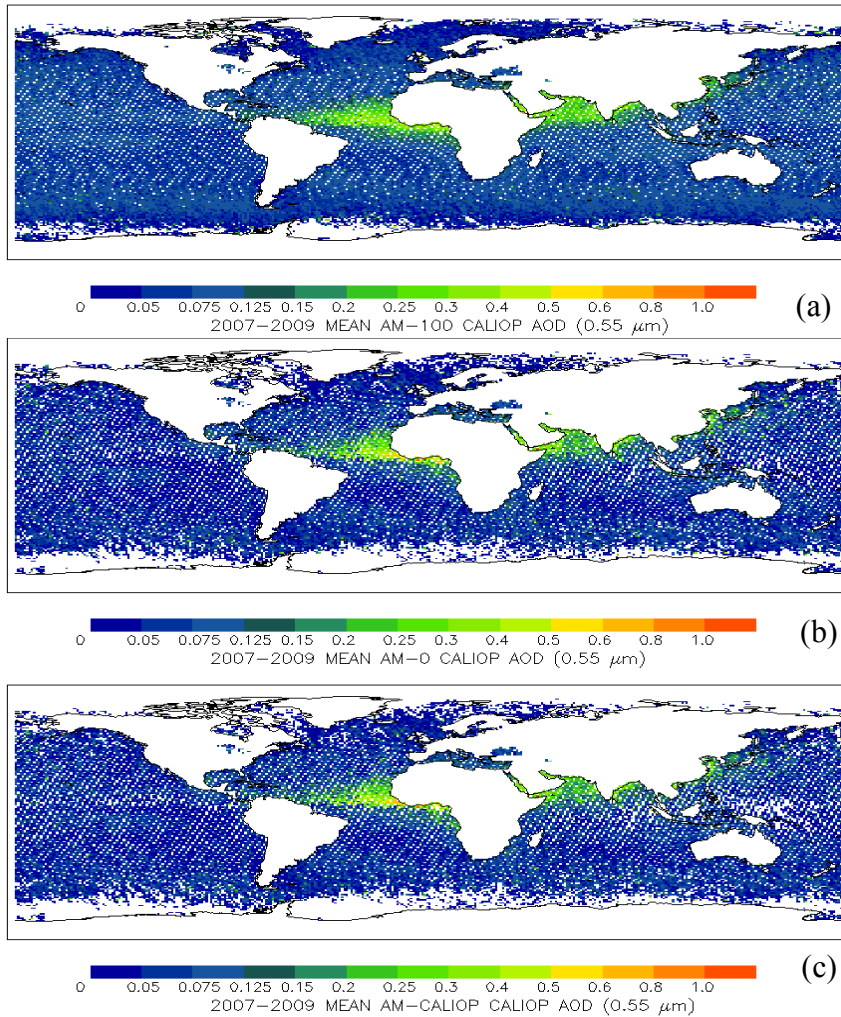


Figure 15. From 2007-2009, (a) AM-100, (b) AM-0 and (c) AM-CALIOP global mean CALIOP AOD for the CALIOP\_Aerosol subset analysis at  $1.0^\circ \times 1.0^\circ$  resolution.

L2\_05kmAProf QA screening removes roughly 20% of the data found from the CALIOP\_Cloud sample, both globally and over the Southern Oceans. Qualitatively, very little change is apparent across each subset analysis. Consistent with Fig. 1d, however, ESOA is not readily apparent in CALIOP-derived mean AOD at any stage of cloud screening. CALIOP algorithms do not detect any significant ESOA structure (e.g., the contrast of zonal averaged AOD between 40°S to 60° S and 20°S to 40° S greater than 0.03 at 0.550  $\mu\text{m}$ ).

Shown in Fig. 16a are zonal mean AOD averages between 60° S and 60° N at 1° meridional resolution for coincident AM and CALIOP data points from the CALIOP\_Aerosol subset, respectively, for the AM-100, AM-0, and AM-CALIOP samples.



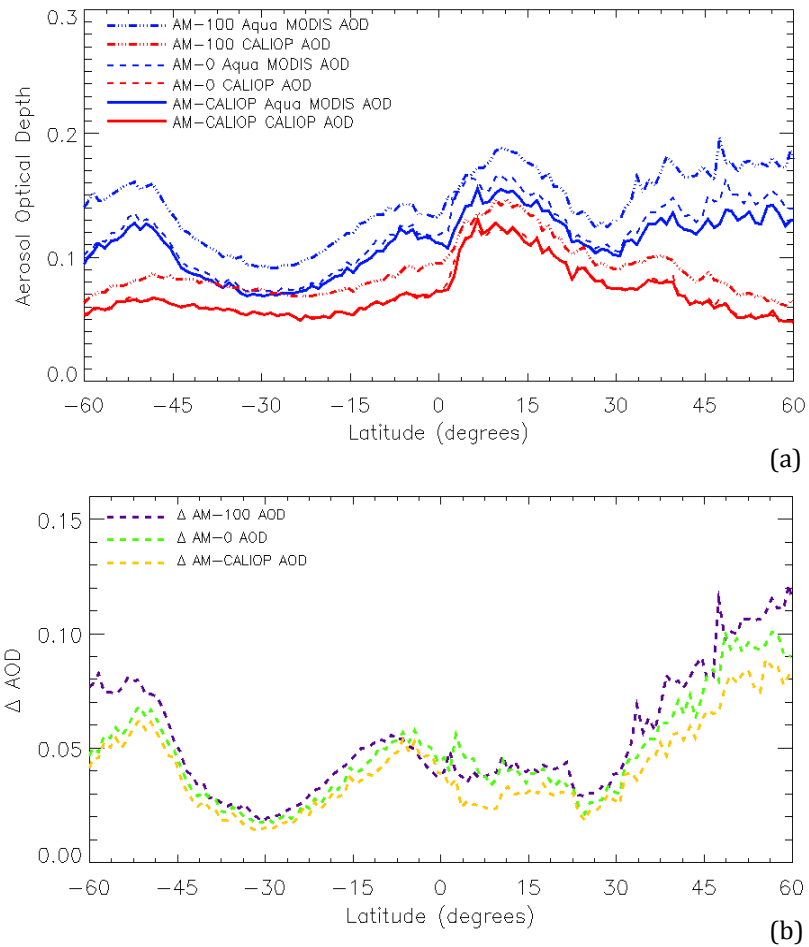


Figure 16. Three-year (2007-2009) global zonal mean of (a) Aqua MODIS AOD (in blue) and the respective CALIOP AOD (in red) for the CALIOP\_Aerosol subset analysis, and (b) the AOD differences between Aqua MODIS and CALIOP for AM-100 (in purple), AM-0 (in green), and AM-CALIOP (in yellow).

Consistent with the CALIOP\_Cloud subset, mean zonal AOD drops with each successive layer of MODIS and then CALIOP L2\_VFM cloud screening. AOD peaks are observed from the MODIS datasets over the Southern Oceans, and the tropical and high-latitude Northern Hemisphere. In contrast, CALIOP AODs are relatively constant in the Southern Hemisphere, peak accordingly in the Northern Hemisphere tropics, and then conspicuously decline continuing along toward higher latitudes. Most importantly,

however, it is clear from this analysis that supplemental CALIOP cloud screening does not suppress ESOA in the CALIOP zonal mean (difference between the solid and dashed red lines).

Shown in Fig. 16b are corresponding differences between AM and CALIOP mean zonal AOD for each sample analysis. The highest offsets between the passive and active instruments are found nearest the poles. However, much of the northern hemisphere includes land surfaces between 30° and 60° N, a region where maximum offsets are derived and pollution plumes exist. Therefore, results over the Southern Oceans region stand out, as it lacks these significant and variable (i.e., not sea salt alone) surface particle sources zonally. Although similar issues also exist over the high latitude northern hemisphere, the existence of transported aerosol plumes from major pollution sources such as Asia, Europe, and North America complicate the issue and thus this discussion is not pursued further.

Figure 17 depicts the relationship between changes to CALIOP cloud fraction (defined here as the relative occurrence frequency of cloudy profiles versus clear ones) and corresponding differences in mean AM and CALIOP AOD between the AM-100 and AM-0 datasets. Each data point represents a 1° zonal average of these two parameters for the Southern Oceans domain. Because the differences in the zonal averages come from samples of differing size, no error bars are shown.

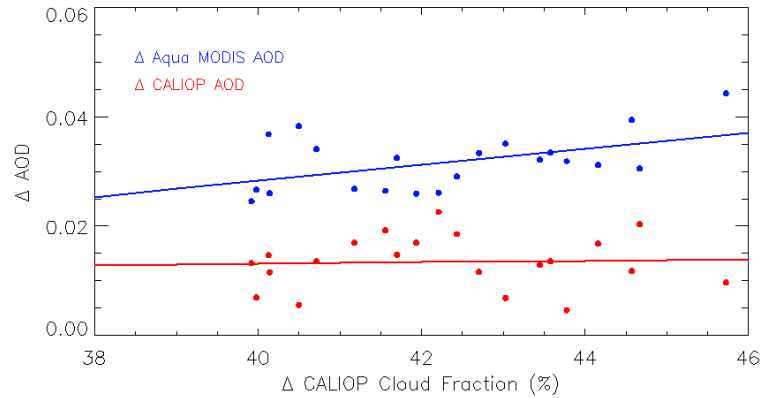


Figure 17. Scatter plot of the change in zonal mean CALIOP cloud fraction (as determined from the VFM) versus the change in zonal mean Aqua MODIS AOD from the AM-100 and AM-0 CALIOP\_Aerosol subset analyses.

Little change is apparent between the difference in mean zonal CALIOP AOD and fraction of VFM cloudiness reduced as a function of MODIS screening. The positive slope, however, apparent from the AM sample, represents a weak correlation ( $R^2 = 0.24$ ) between cloud fraction and the passive sensor AOD estimates. That is, the change in CALIOP cloud fraction introduces a change in zonal mean MODIS AOD but not CALIOP AOD, indicating potential cloud contamination over the ESOA region for MODIS.

Relative differences in AM and CALIOP AOD are next interpreted with respect to L2\_VFM scene and cloud classification. Beginning with the AM-100 analysis (Fig. 18), Fig. 18a depicts the frequency of occurrence for each layer classification category within the Southern Oceans domain, similar to Fig. 6a, though now paired with respective mean AM and CALIOP-derived AOD.

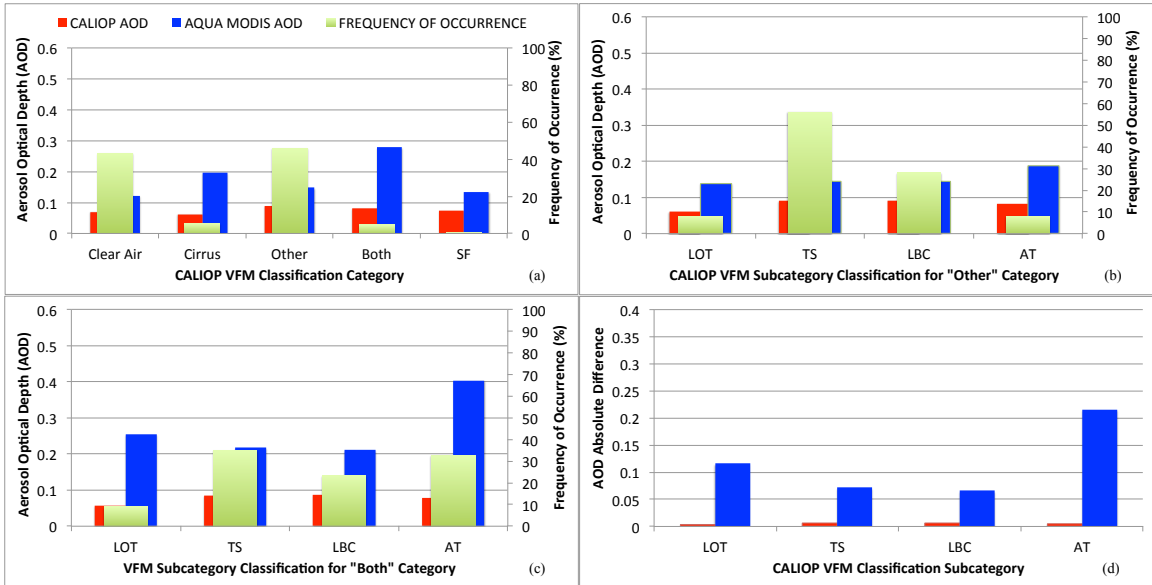


Figure 18. Three-year (2007-2009) average frequency of occurrence of (a) VFM classification categories, (b) “Other” subcategory classification, and (c) “Both” subcategory classification, and their respective Aqua MODIS and CALIOP AOD for the AM-100 CALIOP\_Aerosol subset analysis for the Southern Oceans. Fig. (d) depicts the differences in Aqua MODIS and CALIOP AOD between the “Other” and “Both” subcategories.

Consistent with Fig. 9, the most prevalent scenario identified with CALIOP is Other, or liquid water clouds. Again, this scenario is unique to the Southern Oceans. Interestingly, MODIS AODs are higher for Cirrus cases than Other cases, and the differences between MODIS and CALIOP are relatively larger. This is even true when compared to the limited sample of SF cases.

To distinguish what liquid water cloud types (i.e., phenomenology) are being identified from CALIOP within the AM-100 CALIOP\_Aerosol subset, and thus for cases classified as Other and Both, respectively, Figs. 18b and c include occurrence frequencies and corresponding mean AM and CALIOP AOD for the four most frequent cases of designated VFM cloud type occurrence (the remaining cloud types are observed at very low frequencies, and not shown). Relative AOD differences from each sensor for each

classification are shown in Fig. 18d. Since mean AM and CALIOP AOD for Other cases are generally higher than for cases of Both, the differences in this figure relate to the corresponding value for Other subtracted from that of Both. TS clouds are most commonly identified when the scene is classified as Other, totaling over 50% of the sample. LBC is second, near 30%, and LOT is third at about 10%.

The process is repeated in Fig. 19, now for the AM-0 cloud residual.

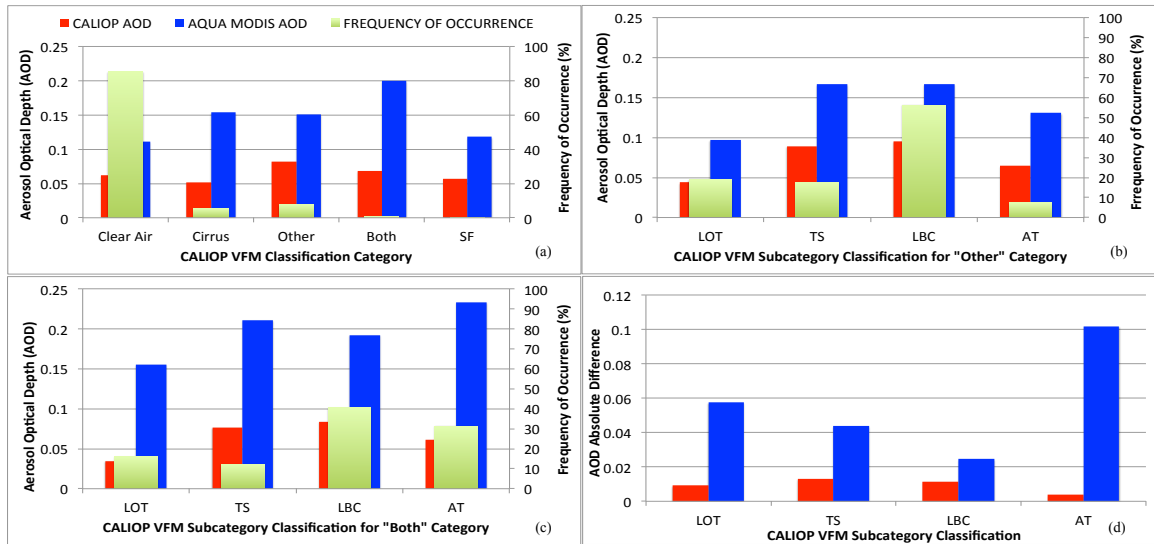


Figure 19. Three-year (2007-2009) average frequency of occurrence of (a) VFM classification categories, (b) “Other” subcategory classification, and (c) “Both” subcategory classification, and their respective Aqua MODIS and CALIOP AOD for the AM-0 CALIOP\_Aerosol subset analysis for the Southern Oceans. Fig. (d) depicts the differences in Aqua MODIS and CALIOP AOD between the “Other” and “Both” subcategories.

Here, however, and as seen above from Fig. 10, most of the cloudiness is suppressed. Cases of Other and Cirrus number about the same, while cases of Both and SF become very small. A change, though, in the type of clouds identified from the L2\_VFM product occurs. For cases of Other, LBC cases now represent nearly 60% of the residual, though TS and LOT sum to about 40% combined. This change is primarily due to the reduction of TS cases from MODIS screening, as both LOT and LBC effectively double in relative

frequency. AOD differences between Other and Both are similar to the AM-100 analysis for TS and LBC, though they are less for LOT and AT.

CALIOP algorithms distinguish between these three primary cloud types as a function of spatial persistence, quantified as a cloud fraction parameter solved from the relative number of clouds identified in 1 km segments with a top height below 3 km along an 80 km segment (Liu et al. 2005). Each type corresponds with a cloud top height pressure above 680 hPa, and is transparent (i.e., the Earth's surface is detected below the apparent cloud base). LOT cases are those where cloud fraction exceeds 0.98 (i.e., clouds detected in at least 79 of 80 1-km profiles in a continuous 80-km segment). TS clouds are those where cloud fraction is less than 0.98 and exceeds 0.40 (approx. mean value  $\sim 0.7$ ). LBC clouds are those where cloud fraction is less than 0.40 (approx. mean value  $\sim 0.2$ ). Therefore, the decrease in TS cases between AM-100 and AM-0 is consistent with MODIS algorithms exhibiting greater efficacy for distinguishing cloud presence for scenes with greater cloud fraction. For LOT, however, MODIS algorithm issues discriminating relatively warm clouds from the ocean surface below likely explain why those relative frequencies actually increase between the AM-100 and AM-0 analyses (e.g., Frey et al. 2008).

Since each of these three layer types may be transparent, this may represent some undersampling in the CALIOP\_Aerosol analysis from the requirement of a valid CALIOP AOD retrieval corresponding with a collocated AM data point. For “low overcast, opaque” clouds, unless there is significant aerosol particle scattering above the cloud, and considering that full pulse attenuation occurs at some point within the cloud inhibiting sampling of an aerosol particle layer below it, these cases are being screened

out in an unrepresentative manner. Comparing Figs. 8 and 16a, the AM-CALIOP AOD analysis for CALIOP\_Cloud is slightly lower than that of CALIOP\_Aerosol, which is likely attributable to this effect. This impact, however, is still low relative to the apparent ESOA offset from CALIOP\_Aerosol (Fig. 16a), as a whole.

### *Spatial Representativeness Analysis*

As discussed in the previous chapter, CALIOP cloud screening of the AM data is incomplete relative to the statistical probability that the lidar actually coincides with a cloud, and thus TS and LBC clouds are undersampled. Therefore, the AM-CALIOP AM AOD profile shown in Fig. 16a can be renormalized based on relative incidence rates and mean respective AOD at 1° meridional resolution to compensate for this undersampling. The renormalized AM-CALIOP AM AOD global profile, computed using Equation 5 from Chapter 2, is shown in Fig. 20. The New AOD 1 line represents the renormalized AM-CALIOP AM AOD based on mean values of AM AOD for LBC and TS for the entire Southern Oceans region. New AOD 2 uses zonal mean values of AM AOD for these two cloud types, and these vary with latitude.

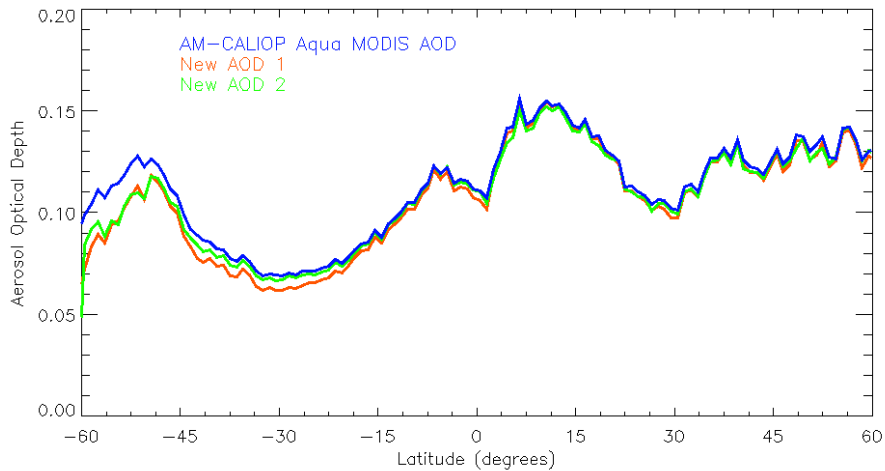


Figure 20. Three-year (2007-2009) global zonal mean of AM-CALIOP Aqua MODIS AOD from the CALIOP\_Aerosol analysis. Original is in dark blue and the corresponding renormalized AOD is in orange and green (based on slightly different AOD averaging schemes).

Little difference is found in the new result globally, except over the Southern Oceans domain. However, even with these most stringent cloud-screening methods applied, a relative spike in zonal mean AOD is still observed over the Southern Oceans between AM (Fig. 20) and CALIOP (Fig. 16a). Though cloud contamination is clearly a factor in ESOA, it does not appear to be the sole contributor, and thus CALIOP screening alone cannot eliminate the ESOA feature in AM datasets.

### *Seasonal Analysis*

For the analysis presented in this work thus far, only annual statistics are shown. Some seasonality exists, however, between summer and winter composite results, as shown in Fig. 21.



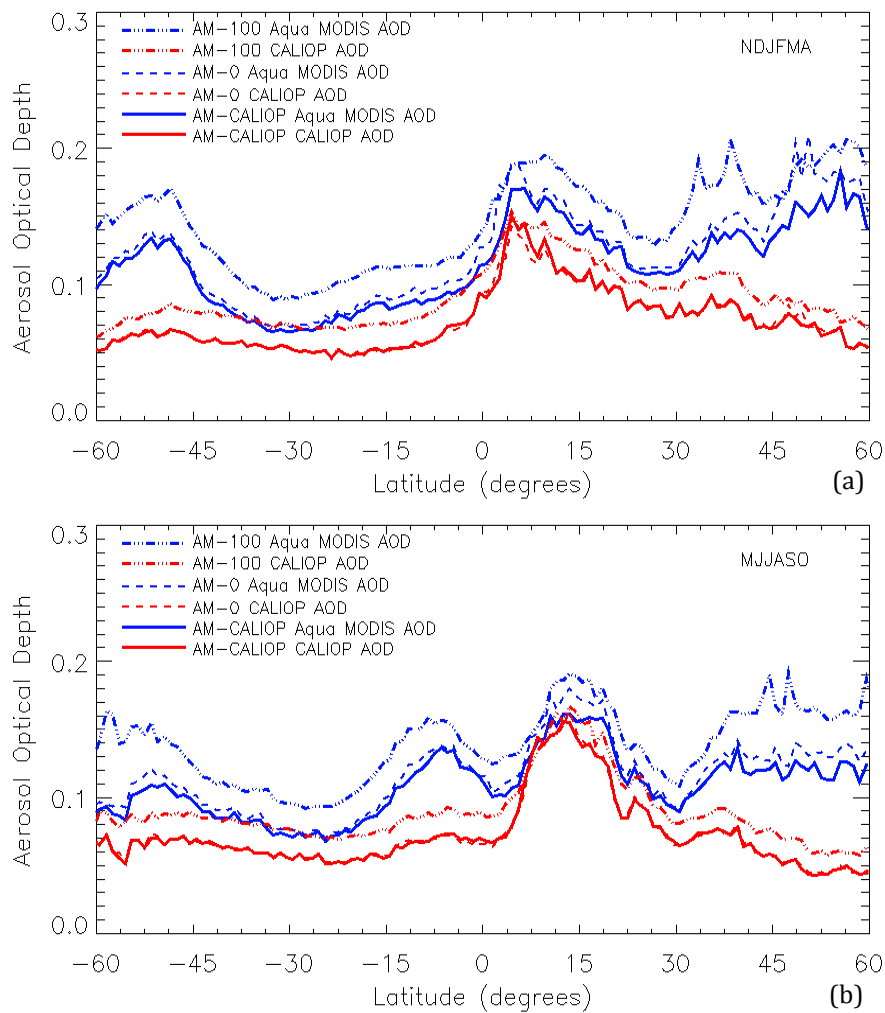


Figure 21. Three-year (2007-2009) global zonal mean of Aqua MODIS AOD (in blue) and the respective CALIOP AOD (in red) for the southern hemisphere (a) summer months (November through April, or NDJFMA) and (b) winter months (May through October, or MJJASO).

ESOA is evident during the southern hemisphere summer months, November through April (NDJFMA). However, this relative spike in AM AOD is not as apparent for the southern hemisphere winter months, May through October (MJJASO). The total number of data samples (shown in Table 5) during Southern Hemisphere winter over the Southern Oceans domain is very limited, though, complicating this analysis. As such, the

influence of cloud contamination on ESOA cannot be significantly decoupled during this period in order to evaluate whether or not there are any relative decreases in AM AOD over the Southern Oceans that are seasonally based. Given that ESOA reflects a potential passive sensor artifact, the ability to detect it is a function of the number of total available data points from the relevant domain, for which winter sample sizes are much lower than that of summer (Table 5). Therefore, the seasonality of ESOA is not investigated further.

Table 5. For the CALIOP\_Aerosol analysis, data counts in the Southern Oceans region for each subset analysis (AM-100, AM-0, and AM-CALIOP) for the southern hemisphere summer months (November through April, or NDJFMA) and winter months (May through October, or MJJASO) are reported.

Product Name	Southern Oceans Data Counts	
	Summer (NDJFMA)	Winter (MJJASO)
AM-100	400,289	184,562
AM-0	97,843	36,231
AM-CALIOP	83,878	31,144

#### *A Case Study*

For a more specific look into the collocated AM/CALIOP datasets, several visible AM images are checked visually for the presence of clouds CALIOP detected in the AM-0 sample. As an example, Fig. 22 shows a case in which CALIOP detected TS clouds in the AM-0 dataset, occurring on January 12<sup>th</sup>, 2009 at 15:26 UTC at (-50.6°, -18.7°). Figure 22a shows the visible image of AM, where the red line indicates the CALIOP track, the blue box shows the 10x10 km AM-0 retrieval, and the black arrow points to the midpoint of the 5 km CALIOP segment focused on in this case study. No clouds are apparent in the AM-0 retrieval. Figure 22b is the matching AM AOD spatial plot,, which shows AOD of about 0.3 at the point in question. From an active standpoint, the CALIOP VFM plot shown in Fig. 22c indicates the presence of clouds (TS) at the point being focused on (black arrow). Lastly, Fig. 22d shows the AM and CALIOP AOD,

~0.3 and ~0.06 respectively, as well as the AM cloud fraction (0%). The lines cease around  $-51.1^\circ$  latitude, for lack of available data.

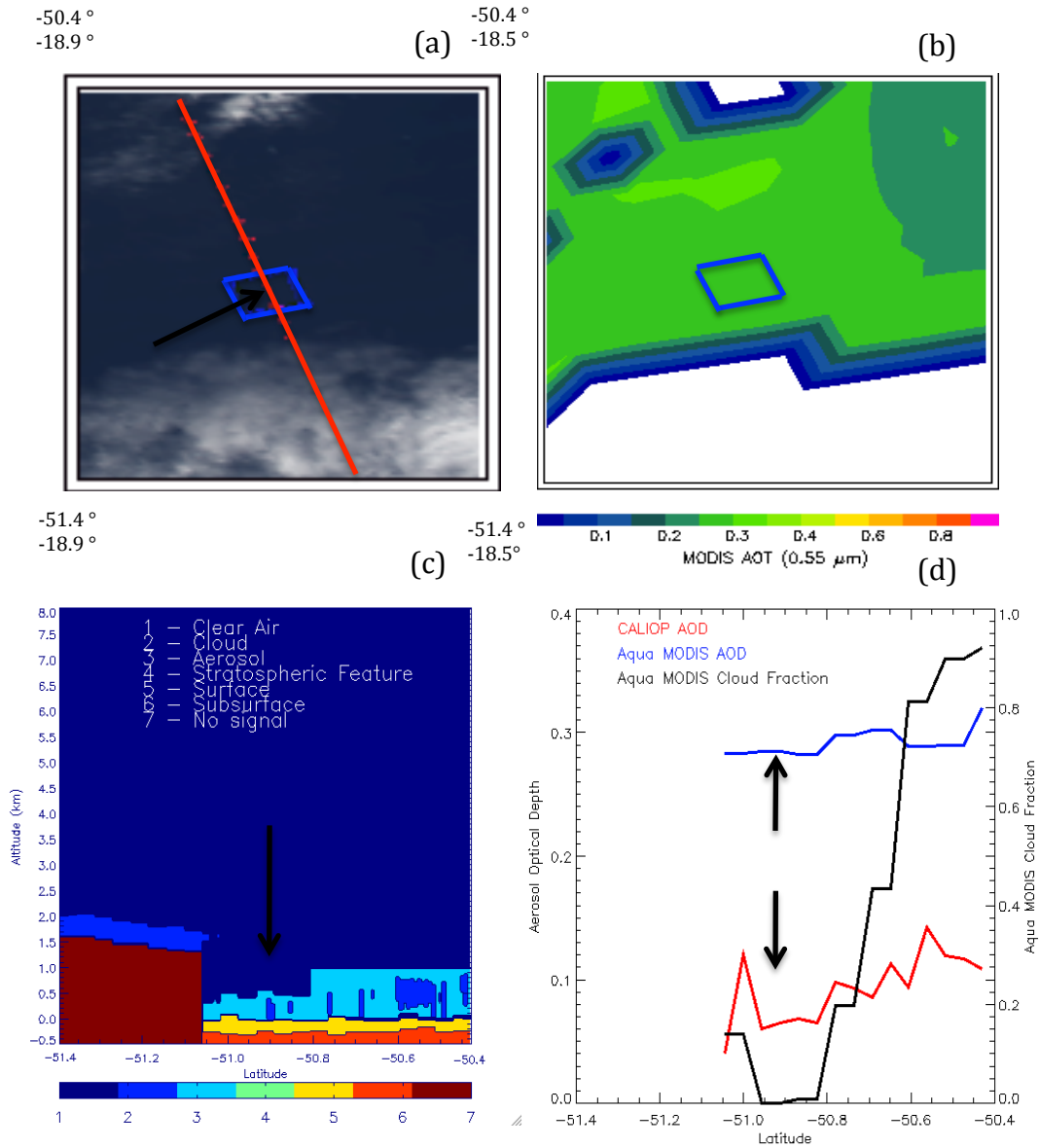


Figure 22. Case study of a collocated Aqua MODIS (AM) and CALIOP point ( $-50.6^\circ$ ,  $-18.7^\circ$ ) on January 12<sup>th</sup>, 2009 at 15:26 UTC. A visible image of AM is shown in (a), where the red line indicates the CALIOP track, the blue box shows the 10x10 km AM-0 retrieval, and the black arrow points to the midpoint of the 5 km CALIOP segment. (b) The corresponding AM AOD spatial plot. (c) CALIOP Vertical Feature Mask (VFM) plot. (d) Line plot of AM AOD, AM cloud fraction, and CALIOP AOD.

While the CALIOP VFM detects TS clouds, the AM image suggests otherwise, as no clouds are visible in the 10x10 km AM-0 retrieval. In fact, the spatial distribution of AM AOD shows a decrease in AOD closer to the edges of clouds in the visible image. Therefore, there may be other explanations (besides cloud contamination) for the elevated AOD observed in this region. Whether or not these are valid observations (possibly from a transported plume) or a retrieval error is not conclusive from this study. Further investigation into this topic is necessary.

## CHAPTER IV

### SUMMARY AND CONCLUSIONS

This thesis analyzes aerosol optical depth (AOD) retrievals from NASA Collection 5 Aqua Moderate Resolution Imaging SpectroRadiometer (AM; 10 km x 10 km mean value; 0.550  $\mu\text{m}$ ) collocated with Maritime Aerosol Network (MAN; 0.550  $\mu\text{m}$ -interpolated), Aerosol Robotic Network (AERONET; 0.550  $\mu\text{m}$ -interpolated) and Version 3.01 Cloud-Aerosol Lidar with Orthogonal Polarization (CALIOP; 5 km along-track average; 0.532  $\mu\text{m}$ ), datasets over the mid to high latitude Southern Oceans (defined as 45° S - 65° S) for an investigation of elevated passive satellite values, referred to as the Elevated Southern Oceans Anomaly (ESOA). The study of this phenomenon is important, as this work shows values of AM AOD (attributed to ESOA) are much higher than the 0.01 benchmark set forth by the climate science community (e.g., Chylek et al. 2003). AM data are evaluated at multiple stages of cloud clearing, including MODIS algorithm cloud fraction estimates and comparison with CALIOP Level 2 Cloud Layer and Vertical Feature Mask datasets, in order to determine whether or not ESOA is the result of cloud contamination.

First, MAN and AERONET data are analyzed against AM AOD retrievals to establish ground-based context for evaluating the presence of ESOA in some passive satellite retrievals over cloud free skies. AM AOD is, on average, higher than MAN and AERONET by about 0.03. Statistically, if ESOA exists, its presence should be apparent from this multi-year analysis of ground-based data. However, this study shows that over

cloud free skies, ESOA does not exist in MAN and AERONET data. This is possibly due to two reasons. For one, the ESOA phenomenon may not exist under cloud free skies over the Southern Oceans. Secondly, the current ground-based observations may have a sampling bias (due to the lack of measurements taken during heavy seas and/or summer hemisphere winter) and missed the scenarios for which ESOA could occur.

Next, the high spatial and vertical resolutions of CALIOP cloud detection capabilities are exploited to investigate whether or not this phenomenon is caused by cloud contamination. From this analysis, it is concluded that cloud screening can significantly reduce ESOA (by 0.031), indicating that some of the ESOA signal can be attributed to unfiltered clouds. The largest contributors to cloud contamination are found to be stratocumulus and low broken cumulus clouds. Also, a weak positive relationship is found between the change in AM AOD and that of CALIOP cloud fraction, which further suggests that cloud contamination exists in the retrieval process of some passive satellites over the Southern Oceans region. However, even with the most stringent cloud screening (correcting for the spatial unrepresentativeness of CALIOP), ESOA is not completely removed from AM datasets.

Through the use of CALIOP data, this study also investigates the cloud types that most commonly pass through MODIS cloud screening algorithms. For the Southern Oceans region, liquid water phase clouds are the largest contributor to this residual cloudiness. This may be due to the large ocean coverage along this band, and possibly marine-type cloudiness. However, across all other areas of the globe, cirrus clouds are the most common type of residual cloud. This suggests the MODIS cloud screening

algorithms are more effective in identifying and eliminating liquid water clouds than cirrus clouds.

Since passive retrievals are based on indirect and multi-spectral techniques, identifying the physical mechanisms causing scenarios like ESOA is necessary for developing more robust algorithms. The skill of global visibility forecasting and mass transport modeling, and in particular those systems dependent on multi-variate satellite data assimilation, is a function of the accuracy and representativeness of those inputs used for initialization (Zhang et al. 2008). Therefore, the ESOA scenario has implications for global aerosol observational and modeling systems, as evident in a recent study of mean AOD global distributions and annual trends (Zhang and Reid 2010). If not properly screened and accounted for, potential signal artifacts, such as ESOA, can potentially induce unnecessary error that negatively impacts any conclusions identified. Although this study shows that even active-based CALIOP screening does not remove this artifact alone, some improvement is still significant. Further, the distinguishing of cloud types most often missed by MODIS screening over open oceans has positive ramifications for improvements to these techniques globally.

Finally, it is important to note that, while this work concludes cloud contamination plays a role in the presence of ESOA, it is not the only cause of this phenomenon. Therefore, several related topics are possible for future study. For one, the band of elevated AM AOD may also be due to surface issues and wind speed effects (e.g., white caps; Lehahn et al. 2010; Madry et al. 2011). However, the next data release for MODIS (Collection 6) may help alleviate the ESOA problem in this regard, as the new algorithms will include an improved multi-wind speed look up table (Kleidman et al. 2012). It will

be interesting to investigate ESOA with these new data, and discover how much ESOA is reduced, if it is at all. Other possible causes of ESOA are inaccurate aerosol models and under/overestimated ocean surface albedo values used in the MODIS retrieval process (e.g., Shi et al. 2011), cloud-sidescattering effects (e.g. Zhang and Reid 2006; Wen et al. 2007; Marshak et al. 2008), and cloud halos (i.e., the “twilight zone” effect; Koren et al. 2007). These topics, along with surface effects, are ideal material for future studies of ESOA.



## APPENDIX

Appendix A  
Acronyms and Definitions

Acronym	Definition
AERONET	Aerosol Robotic Network
AM	Aqua MODIS
AOD	Aerosol Optical Depth
AT	AltoCumulus (Transparent)
AVHRR	Advanced Very High Resolution Radiometer
CAD Score	Cloud-Aerosol Discrimination Score
CALIOP	Cloud-Aerosol Lidar with Orthogonal Polarization
CALIPSO	Cloud-Aerosol Lidar and Infrared Pathfinder Satellite Observations
CFO	Cloud Fraction Ocean
EODBO	Effective Optical Depth Best Ocean
ESOA	Elevated Southern Oceans AOD
FOV	Field of View
GACP	Global Aerosol Climatology Project
LBC	Low Broken Cumulus
LIDAR	Light Detection and Ranging
LOT	Low Overcast (Transparent)
LUT	Look Up Table
MAN	Maritime Aerosol Network
MISR	Multi-angle Imaging SpectroRadiometer
MJJASO	May through October
MODIS	Moderate Resolution Imaging SpectroRadiometer
MSL	Mean Sea Level
NDJFMA	November through April
PSC	Polar Stratospheric Clouds
QA	Quality Assurance
QAO	Quality Assurance Ocean
RADAR	Radio Detection and Ranging
SeaWiFS	Sea-viewing Wide Field-Of View Sensor
SF	Stratospheric Feature
SS	Sea Salt
TS	Transition Stratocumulus
VFM	Vertical Feature Mask

## REFERENCES

- Ackerman, S. A., R. E. Holz, R. Frey, E. W. Eloranta, B. C. Maddux, M. McGill (2008), Cloud Detection with MODIS. Part II: Validation, *J. Atmos. Oceanic Technol.*, 25, 1073–1086.
- Anderson, T., R. J. Charlson, S. E. Schwartz, R. Knutti, O. Boucher, H. Rodhe, and J. Heintzenberg (2003), Climate forcing by aerosols: A hazy picture, *Science*, 300, 1103–1104.
- CALIPSO Data Products Catalog (2006). Retrieved December 5, 2012 from [http://www-calipso.larc.nasa.gov/products/CALIPSO\\_DPC\\_Rev2x3.pdf](http://www-calipso.larc.nasa.gov/products/CALIPSO_DPC_Rev2x3.pdf).
- CALIPSO Quality Statements (2012). Retrieved December 5, 2012, from [http://eosweb.larc.nasa.gov/PRODOCS/calipso/Quality\\_Summaries/CALIOP\\_L2\\_VFMPProducts\\_3.01.html](http://eosweb.larc.nasa.gov/PRODOCS/calipso/Quality_Summaries/CALIOP_L2_VFMPProducts_3.01.html).
- Campbell, J. R., J. L. Tackett, J. S. Reid, J. Zhang, C. A. Curtis, E. J. Hyer, W. R. Sessions, D. L. Westphal, J. M. Prospero, E. J. Welton, A. H. Omar, M. A. Vaughan, and D. M. Winker (2012), Evaluating nighttime CALIOP 0.532  $\mu\text{m}$  aerosol optical depth and extinction coefficient retrievals, *Atmos. Meas. Tech. Discuss.*, 5, 2747-2794.
- Chew, B. N., J. R. Campbell, J. S. Reid, D. M. Giles, E. J. Welton, S. V. Salinas, and S. C. Liew (2011), Tropical cirrus cloud contamination in sun photometer data, *Atmos. Env.*, 45, 6724-6731.

- Chin M., P. Ginoux, S. Kinne, O. Torres, B. Holben, B. Duncan, R. Martin, J. Logan, A. Higurashi, and T. Nakajima (2002), Tropospheric aerosol optical thickness from the GOCART model and comparisons with satellite and sun photometer measurements, *J. Atmos. Sci.*, 59, 461-483.
- Chylek, P., B. Henderson, and M. Mishchenko (2003), Aerosol radiative forcing and the accuracy of satellite aerosol optical depth retrieval, *J. Geophys. Res.*, 108, 4764.
- Delene, D. J. and Ogren, J. A.: Variability of aerosol optical properties at four North American surface monitoring sites (2002), *J. Atmos. Sci.*, 59, 1135–1150.
- Diner, D. J., J. C. Beckert, T. H. Reilly, C. J. Bruegge, J. E. Conel, R. A. Kahn, J. V. Martonchik, T. P. Ackerman, R. Davies, S. A. W. Gerstl, H. R. Gordon, J.-P. Muller, R. B. Myneni, P. J. Sellers, B. Pinty, M. M. Verstraete (1998), Multi-angle Imaging SpectroRadiometer (MISR) instrument description and experiment overview, *IEEE Trans. Geosci. Remote Sens.*, 36, 1072-1087.
- Frey, R. A., S. A. Ackerman, Y. Liu, K. I. Strabala, H. Zhang, J. R. Key, and X. Wang (2008), Cloud detection with MODIS. Part I: Improvements in the MODIS Cloud Mask for Collection 5, *J. Atmos. Oceanic Technol.*, 25, 1057-1072.
- Gao, B. C., P. Yang, W. Han, R. R. Li, and W. J. Wiscombe (2002), An algorithm using visible and 1.38-mm channels to retrieve cirrus cloud reflectances from aircraft and satellite data, *IEEE Trans. Geosci. Remote Sens.*, 40(8), 1659-1668.
- Gathman, S. G. (1983), Optical properties of the marine aerosol as predicted by the Navy aerosol model, *Opt. Eng.*, 22, 57–63.
- Gedzelman, S. D. (1988), In praise of altocumulus, *Weatherwise*, 41, 143–149.

- Holben B.N., T.F. Eck, I. Slutsker, D. Tanré, J.P. Buis, A. Setzer, E. Vermote, J.A. Reagan, Y. Kaufman, T. Nakajima, F. Lavenu, I. Jankowiak, and A. Smirnov, (1998), AERONET - A federated instrument network and data archive for aerosol characterization, *Rem. Sens. Environ.*, 66, 1-16.
- Hunt, W. H., D. M. Winker, M. A. Vaughan, K. A. Powell, P. L. Lucker, and C. Weimer (2009), CALIPSO Lidar Description and Performance Assessment, *J. Atmos. Oceanic Technol.*, 26, 1214–1228.
- Hyer, E. J., Reid, J. S., and Zhang, J. (2011), An over-land aerosol optical depth data set for data assimilation by filtering, correction, and aggregation of MODIS Collection 5 optical depth retrievals, *Atmos. Meas. Tech.*, 4, 379-408.
- Jaegle, L., P. K. Quinn, T.S. Bates, B. Alexander, and J.-T. Lin (2011), Global distribution of sea salt aerosols: new constraints from in situ and remote sensing observations, *Atmos. Chem. Phys.*, 11, 3137-3157.
- Kaufman, Y. J., D. Tanré, and O. Boucher (2002), A satellite view of aerosols in the climate system, *Nature*, 419, 215–223.
- Kaufman, Y. J., L. A. Remer, D. Tanré, R. R. Li, R. Kleidman, S. Mattoo, R. Levy, T. Eck, B. N. Holben, C. Ichoku, J. Martins, and I. Koren (2005), A critical examination of the residual cloud contamination and diurnal sampling effects on MODIS estimates of aerosol over ocean, *IEEE Trans. Geosci. Remote Sens.*, 43, 2886–2897.
- Kittaka, C., D. M. Winker, M. A. Vaughan, A. Omar, and L. A. Remer (2011), Intercomparison of column aerosol optical depths from CALIPSO and MODIS-Aqua, *Atmos. Meas. Tech.*, 4, 131–141.

- Kleidman, R.G., A.Smirnov, R.C.Levy, S.Mattoo, and D.Tanre (2012), Evaluation and wind speed dependence of MODIS aerosol retrievals over open ocean, *IEEE Trans. Geosci. Rem. Sens.*, 50, 429-435.
- Koren, I., L. A. Remer, Y. J. Kaufman, Y. Rudich, and J. V. Martins (2007), On the twilight zone between clouds and aerosols, *Geophys. Res. Lett.*, 34, L08805.
- Kreyszig, E. (2006), *Advanced Engineering Mathematics*, Ninth edition, Wiley, 1248 pp.
- Lehahn, Y., I. Koren, E. Boss, Y. Ben-Ami, and O. Altaratz (2010), Estimating the maritime component of aerosol optical depth and its dependency on surface wind speed using satellite data, *Atmos. Chem. Phys.*, 10, 6711-6720.
- Lewis, E. R. and Schwartz, S. E. (2004), *Sea Salt Aerosol Production: Mechanisms, Methods, Measurements, and Models - A Critical Review*, Geophysical Monograph Series Vol. 152, American Geophysical Union.
- Liu, Z., A. H. Omar, Y. Hu, M. A. Vaughan, and D. M. Winker (2005), CALIOP Algorithm Theoretical Basis Document - Part 3: Scene Classification Algorithms, PC-SCI-202.03, NASA Langley Research Center, 56 pp.
- Madry, W. L., O. B. Toon, and C. D. O' Dowd (2011), Modeled optical thickness of sea-salt aerosol, *J. Geophys. Res.*, 116, D08211.
- Marshak, A., G. Wen, J. A. Coakley Jr., L. A. Remer, N. G. Loeb, and R. F. Cahalan (2008), A simple model for the cloud adjacency effect and the apparent bluing of aerosols near clouds, *J. Geophys. Res.*, 113, D14S17.
- Menon, S., J.E. Hansen, L. Nazarenko, and Y. Luo (2002), Climate effects of black carbon Aerosols in China and India, *Science*, 297, 2250-2253.

- Mishchenko, M., Geogdzhayev, I., Rossow, W., Cairns, B., Carlson, B., Lacis, A., Liu, L., and L.D. Travis (2007), Long-term satellite record reveals likely recent aerosol trend, *Science*, 315(5818), 1543–1543.
- Murphy, D. M., J. R. Anderson, P. K. Quinn, L. M. McInnes, F. J. Brechtel, S. M. Kreidenweis, A. M. Middlebrook, M. Posfai, D. S. Thomson, and P. R. Buseck (1998), Influence of sea-salt on aerosol radiative properties in the Southern Ocean marine boundary layer, *Nature*, 392, 62–65.
- Myhre, G., Stordal, F., Johnsrud, M., Ignatov, A., Mishchenko, M. I., Geogdzhayev, I. V., Tanré, D., Deuzé, J.-L., Goloub, P., Nakajima, T., Higurashi, A., Torres, O., and Holben, B. (2004), Intercomparison of satellite retrieved aerosol optical depth over the ocean, *J. Atmos. Sci.*, 61, 499-513.
- Myhre, G., Stordal, F., Johnsrud, M., Diner, D. J., Geogdzhayev, I. V., Haywood, J. M., Holben, B. N., Holzer-Popp, T., Ignatov, A., Kahn, R. A., Kaufman, Y. J., Loeb, N., Martonchik, J. V., Mishchenko, M. I., Nalli, N. R., Remer, L. A., Schroedter-Homscheidt, M., Tanré, D., Torres, O., and Wang, M. (2005), Intercomparison of satellite retrieved aerosol optical depth over ocean during the period September 1997 to December 2000, *Atmos. Chem. Phys.*, 5, 1697-1719.
- Omar, A. H., D. M. Winker, C. Kittaka, M. A. Vaughan, Z. Liu, Y. Hu, C. Trepte, R. R. Rogers, R. A. Ferrare, K.-P. Lee, R. E. Kuehn, and C. A. Hostetler (2009), The CALIPSO Automated Aerosol Classification and Lidar Ratio Selection Algorithm, *J. Atmos. Oceanic Technol.*, 26, 1994-2014.
- Pope, CA III (2004), Air pollution and health – Good news and bad, *N. Engl. J. Med.*, 351, 1132-1134.

- Purkis, S. J., & Klemas, V. (2011), *Remote sensing and global environmental change*, Wiley-Blackwell, 384 pp.
- Ramanathan, V., P. J. Crutzen, J. T. Kiehl, and D. Rosenfeld (2001), Aerosols, climate and the hydrological cycle, *Science*, 294, 2119-2124.
- Rao, C. R. N., L. L. Stowe, and E. P. McClain (1989), Remote sensing of aerosols over the oceans using AVHRR data: theory, practice and applications, *Int. J. Remote Sens.*, 10, 743-749.
- Remer, L. A., Y. J. Kaufman, D. Tanre', S. Mattoo, D. A. Chu, J. V. Martins, R.-R. Li, C. Ichoku, R. C. Levy, R. G. Kleidman, T. F. Eck, E. Vermote, and B. N. Holben (2005), The MODIS aerosol algorithm, products, and validation, *J. Atmos. Sci.*, 62, 947–973.
- Sassen, K., and B. S. Cho (1992), Subvisual-thin cirrus lidar dataset for satellite verification and climatological research, *J. Appl. Meteor.*, 31, 1275–1285.
- Sassen, K., and J. R. Campbell (2001), A remote sensing midlatitude cirrus cloud climatology: I. Macrophysical and synoptic properties, *J. Atmos. Sci.*, 58, 481-496.
- Sayer, A. M., N. C. Hsu, C. Bettenhausen, Z. Ahmad, B. N. Holben, A. Smirnov, G. E. Thomas, and J. Zhang (2012), SeaWiFS Ocean Aerosol Retrieval (SOAR): algorithm, validation, and comparison with other datasets, *J. Geophys. Res.*, 117, D03206.



- Schuster, G. L., Vaughan, M., MacDonnell, D., Su, W., Winker, D., Dubovik, O., Lapyonok, T., Trepte, C. (2012), Comparison of CALIPSO aerosol optical depth retrievals to AERONET measurements, and a climatology for the lidar ratio of dust, *Atmos. Chem. Phys. Discuss.*, 12, 11641– 11697.
- Shi, Y., J. Zhang, J. S. Reid, B. Holben, E. J. Hyer, and C. Curtis (2011), An analysis of the Collection 5 MODIS over-ocean aerosol optical depth product for its implication in aerosol assimilation, *Atmos. Chem. Phys.*, 11, 557-565.
- Smirnov, A., B. N. Holben, D. M. Giles, I. Slutsker, N. T. O'Neill, T. F. Eck, A. Macke, P. Croot, Y. Courcoux, S. M. Sakerin, T. J. Smyth, T. Zielinski, G. Zibordi, J. I. Goes, M. J. Harvey, P. K. Quinn, N. B. Nelson, V. F. Radionov, C. M. Duarte, R. Losno, J. Sciare, K. J. Voss, S. Kinne, N. R. Nalli, E. Joseph, K. Krishna Moorthy, D. S. Covert, S. K. Gulev, G. Milinevsky, P. Larouche, S. Belanger, E. Horne, M. Chin, L. A. Remer, R. A. Kahn, J. S. Reid, M. Schulz, C. L. Heald, J. Zhang, K. Lapina, R. G. Kleidman, J. Griesfeller, B. J. Gaitley, Q. Tan, and T. L. Diehl (2011), Maritime Aerosol Network as a component of AERONET – first results and comparison with global aerosol models and satellite retrievals, *Atmos. Meas. Tech.*, 4, 583-597.
- Stephens, G.L., D.G. Vane, R.J. Boain, G.G. Mace, K. Sassen, Z. Wang, A.J. Illingworth, E.J. O'Connor, W.B. Rossow, S.L. Durden, S.D. Miller, R.T. Austin, A. Benedetti, C. Mitrescu, and CloudSat Science Team (2002), The CloudSat mission and the A-Train: A new dimension of space-based observations of clouds and precipitation, *Bull. Amer. Meteorol. Soc.*, 83, 1771-1790.

- Vaughan, M. A., K. A. Powell, R. E. Kuehn, S. A. Young, D. M. Winker, C. A. Hostetler, W. H. Hunt, Z. Liu, M. J. McGill, and B. J. Getzewich (2009), Fully automated detection of cloud and aerosol layers in the CALIPSO lidar measurements, *J. Atmos. Oceanic Technol.*, 26, 2034-2050.
- Wallace J.M. and P.V. Hobbs (2006), *Atmospheric science: an introductory survey* (2nd edition), International Geophysics Series 92, Associated press, 484 pp.
- Wen, G., A. Marshak, R. F. Cahalan, L. A. Remer, and R. G. Kleidman (2007), 3D Aerosol-cloud radiative interaction observed in collocated MODIS and ASTER images of cumulus cloud fields, *J. Geophys. Res.*, 112, D13204.
- Wielicki, B. A., R. D. Cess, M. D. King, D. A. Randall, and E. F. Harrison (1995), Mission to planet earth: Role of clouds and radiation in climate, *Bull. Amer. Meteor. Soc.*, 76, 2125–2153.
- Winker, D. M., W. H. Hunt, and M. J. McGill (2007), Initial performance assessment of CALIOP, *Geophys. Res. Lett.*, 34, L19803.
- Winker, D. M., J. L. Tackett, B. J. Getzewich, Z. Liu, M. A. Vaughan, and R. R. Rogers, (2012), The global 3-D distribution of tropospheric aerosols as characterized by CALIOP, *Atmos. Chem. Phys. Discuss.*, 12, 24847-24893.
- Yorks, J., D. Hlavka, M. Vaughan, M. McGill, W. Hart, S. Rodier, and R. Kuehn (2011), Airborne Validation of Cirrus Cloud Properties Derived from CALIPSO Lidar Measurements: Spatial Properties, *J. Geophys. Res.*, 116, D19207.

- Young, S. A., and M. A. Vaughan (2009), The retrieval of profiles of particulate extinction from Cloud-Aerosol Lidar Infrared Pathfinder Satellite Observations (CALIPSO) data: algorithm description, *J. Atmos. Oceanic Technol.*, 26, 1105-1119.
- Yu H., R. Dickinson, M. Chin, Y. Kaufman, B. Holben, I. Geogdzhayev, and M. Mishchenko (2003), Annual cycle of global distributions of aerosol optical depth from integration of MODIS retrievals and GOCART model simulations, *J. Geophys. Res.*, 108 (D3), 4128.
- Zhang, J., J. S. Reid, and B. N. Holben (2005), An analysis of potential cloud artifacts in MODIS over ocean aerosol optical thickness products, *Geophys. Res. Lett.*, 32, L15803.
- Zhang, J., J. S. Reid, D. L. Westphal, N. L. Baker, and E. J. Hyer (2008), A system for operational aerosol optical depth data assimilation over global oceans, *J. Geophys. Res.*, 113, D10208.
- Zhang, J., and J. S. Reid (2006), MODIS aerosol product analysis for data assimilation: Assessment of over-ocean level 2 aerosol optical thickness retrievals, *J. Geophys. Res.*, 111, D22207.
- Zhang, J., and J. S. Reid (2009), An analysis of clear sky and contextual biases using an operational over ocean MODIS aerosol product, *Geophys. Res. Lett.*, 36, L15824.
- Zhang, J., and J. S. Reid (2010), A decadal regional and global trend analysis of the aerosol optical depth using a data-assimilation grade over-water MODIS and Level 2 MISR aerosol products, *Atmos. Chem. Phys.*, 10, 10949-10963.

Zhang, R.-J., K. F. Ho, and Z.-X. Shen (2012), The role of aerosol in climate change, the environment, and human health, *Atmos. Oceanic Sci. Lett.*, 5, 156–161.